Available online at www.sciencedirect.com

ScienceDirect

Geochimica et Cosmochimica Acta 183 (2016) 106–124

Geochimica et Cosmochimica Acta

www.elsevier.com/locate/gca

The contribution of hydrothermally altered ocean crust to the mantle halogen and noble gas cycles

Déborah Chavrit [a,*], Ray Burgess [a], Hirochika Sumino [b,c], Damon A.H. Teagle [d], Giles Droop [a], Aya Shimizu [b,e], Chris J. Ballentine [a,f]

[a] School of Earth, Atmospheric and Environmental Sciences, University of Manchester, Oxford Road, Manchester M13 9PL, UK
[b] Geochemical Research Center, Graduate School of Science, University of Tokyo, Tokyo 113-0033, Japan
[c] Department of Basic Science, Graduate School of Arts and Sciences, The University of Tokyo, 3-8-1 Komaba, Meguro-ku, Tokyo 153-8902, Japan
[d] Ocean and Earth Science, National Oceanography Centre Southampton, University of Southampton, SO14 3ZH, UK
[e] Tokyo Metropolitan Industrial Technology Research Institute, Tokyo 135-0064, Japan
[f] Department of Earth Sciences, University of Oxford, South Parks Road, Oxford OX1 3AN, UK

Received 24 June 2015; accepted in revised form 12 March 2016; available online 18 March 2016

Abstract

Recent studies suggest that seawater-derived noble gases and halogens are recycled into the deep mantle by the subduction of oceanic crust. To understand the processes controlling the availability of halogens and noble gases for subduction, we determined the noble gas elemental and isotopic ratios and halogen (Cl, Br, I) concentrations in 28 igneous samples from the altered oceanic crust (AOC) from 5 ODP sites in the Eastern and Western Pacific Ocean. Crushing followed by heating experiments enabled determination of noble gases and halogens in fluid inclusions and mineral phases respectively. Except for He and Ar, Ne, Kr and Xe isotopic ratios were all air-like suggesting that primary MORB signatures have been completely overprinted by air and/or seawater interaction. In contrast, $^{3}He/^{4}He$ ratios obtained by crushing indicate that a mantle helium component is still preserved, and $^{40}Ar/^{36}Ar$ values are affected by radiogenic decay in the mineral phases. The $^{130}Xe/^{36}Ar$ and $^{84}Kr/^{36}Ar$ ratios are respectively up to 15 times and 5 times higher than those of seawater and the highest ratios are found in samples affected by low temperature alteration (shallower than 800–900 m sub-basement). We consider three possible processes: (i) adsorption onto the clays present in the samples; (ii) fluid inclusions with a marine pore fluid composition; and (iii) fractionation of seawater through phase separation caused by boiling. Ninety percent of the Cl, Br and I were released during the heating experiments, showing that halogens are dominantly held in mineral phases prior to subduction. I/Cl ratios vary by 4 orders of magnitude, from 3×10^{-6} to 2×10^{-2}. The mean Br/Cl ratio is 30% lower than in MORB and seawater. I/Cl ratios lower than MORB values are attributed to Cl-rich amphibole formation caused by hydrothermal alteration at depths greater than 800–900 m sub-basement together with different extents of I loss during low and high temperature alteration. At shallower depths, I/Cl ratios higher than MORB values can be explained by the addition of organic-rich sediments or the presence of organic detritus, both known to efficiently sequester I. Concentrations of ^{36}Ar of the pre-subducting materials are sufficient to account for the ^{36}Ar and composition of the mantle in the context of existing subduction-flux models. We

* Corresponding author at: Institut de Physique du Globe de Paris, Sorbonne Paris Cité, Univ Paris Diderot, CNRS, F-75005 Paris, France. Tel.: +33 1 83 95 74 41.

E-mail addresses: chavrit@ipgp.fr (D. Chavrit), ray.burgess@manchester.ac.uk (R. Burgess), sumino@igcl.c.u-tokyo.ac.jp (H. Sumino), Damon.Teagle@southampton.ac.uk (D.A.H. Teagle), giles.droop@manchester.ac.uk (G. Droop), shimizu.aya@iri-tokyo.jp (A. Shimizu), chris.ballentine@earth.ox.ac.uk (C.J. Ballentine).

http://dx.doi.org/10.1016/j.gca.2016.03.014
0016-7037/

find the Cl subduction flux of the oceanic crust to be about three times higher than the previous estimates and that sufficient Cl and Br can potentially be delivered by subduction over the last 3 Ga to account for mantle source compositions.

1. INTRODUCTION

Noble gases have played a central role in developing models of mantle convection and geochemical evolution (Porcelli and Ballentine, 2002; Moreira, 2013). Early models of a layered mantle with different convection regimes, separated by the 670 km phase change (e.g. Allègre et al., 1983; Kaneoka, 1983; O'Nions and Oxburgh, 1983; Porcelli and Wasserburg, 1995), have been challenged by deep Earth seismic imaging and numerical models of mantle convection using realistic viscosities that favour whole mantle convection (e.g. van der Hilst et al., 1997; van Keken and Ballentine, 1999). Consequently, we have yet to achieve a coherent view on the sources of volatiles such as water, carbon dioxide, halogens and noble gases in the mantle and their relationship to mantle convection and plate tectonics. A major question is the extent to which volatiles are carried into the deep mantle by subduction and whether this influences the volatile concentrations and therefore the physical and isotopic character of the convecting mantle. A clear understanding of volatile recycling through time is essential if we are to quantify the influence of this process on the isotopic character of Ocean Island and Mid Ocean Ridge systems within the context of whole mantle convection (Holland and Ballentine, 2006; Ballentine and Holland, 2008; Brandenburg et al., 2008).

Early investigations of the mantle volatile system suggested that subduction is an efficient barrier to noble gas recycling. Staudacher and Allègre (1988) for example, argued that "at least 98%" of the noble gases that they estimated to be available for recycling in the downgoing slab are returned to the surface during subduction and arc volcanism. Commonly, this assertion has been interpreted as a complete barrier to noble gas recycling by subduction. In contrast, other studies (Holland and Ballentine, 2006; Ballentine and Holland, 2008; Holland et al., 2009) have shown the elemental composition of heavy noble gas is similar to that of marine pore fluid, and there is an air-like isotopic overprint on primitive heavy noble gases in the mantle. This provides evidence for recycling of atmosphere-derived Ar, Kr and Xe back into the mantle, which has also been recently suggested by Mukhopadhyay (2012) and Parai and Mukhopadhyay (2015).

Further evidence for volatile recycling is provided by combining noble gases with halogen measurements. Halogens (Cl, Br, I) provide an additional and powerful tracer of seawater and sedimentary involvement in the subduction process. In contrast to noble gases, halogens are not affected by atmospheric contamination during recovery or in the laboratory (Sumino et al., 2010). Potential contributors of noble gases and halogens to the mantle are marine sediments, hydrothermally altered ocean crust (AOC), and serpentinised upper mantle peridotites. Marine pore fluid halogen (Cl, Br, I) and noble gas signatures are preserved in peridotites subducted to at least 100 km depth (Sumino et al., 2010), and in serpentinites subducted to depths of up to 70 km (Kendrick et al., 2011, 2013b). It has also been demonstrated that noble gases have a high solubility in amphibole and that these and similar mineral structures, such as serpentinite, may indeed provide a recycling pathway for noble gases into the mantle (Jackson et al., 2013, 2015; Kendrick et al., 2015).

A limited number of studies have considered the noble gas compositions of altered oceanic crust: altered mid-ocean ridge basalts (MORB) (Staudacher and Allègre, 1988, $n = 8$ samples); gabbros (Kumagai et al., 2003, $n = 5$, Moreira et al., 2003 for He and Ne, $n = 10$); and marine sediments (Matsuda and Nagao, 1986, $n = 7$ and Staudacher and Allègre, 1988, $n = 3$). Progress has been impeded by the analytical limitations of measuring the low abundance of Br and I in igneous rocks. Consequently, apart from one recent study reporting Cl, Br and I in mineral separates of oceanic metagabbros (Kendrick et al., 2015), most previous halogen data are restricted to F and Cl determinations (e.g. Sano et al., 2008; Barnes and Cisneros, 2012).We present here a systematic study of noble gases and halogens (Cl, Br and I) in samples of the oceanic crust altered at low and high temperature, in order to identify the lithological, stratigraphic and temporal record of their variations and the respective major host phases in pre-subducted material.

2. ALTERED OCEAN CRUST SAMPLES

Subduction of oceanic crust is dominated by that produced at fast spreading ridges (e.g. Van Keken et al.,

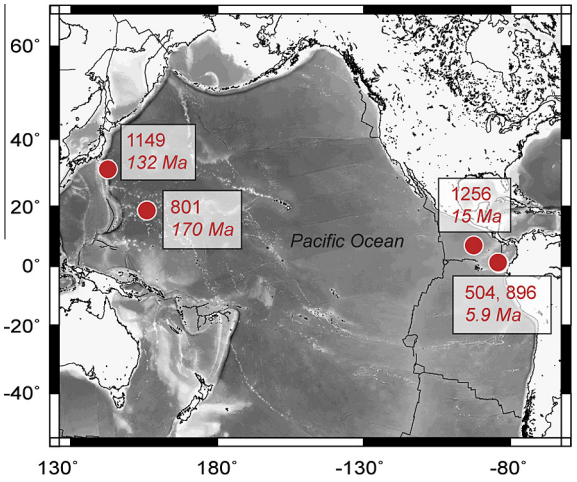

Fig. 1. Location map of the DSDP/ODP sites showing the location of samples.

Table 1
Sample details.

Sample abbr. name	Sample full name	Depth		Sample description	Main 2nd mineral.		NG isotopes analysis
		mbsf	msb		Amph.	Clay	
Altered igneous rocks							
Site 896	*(Lat. 1.22; Lon. -83.72; Age 5.9 Ma; spreading rate 72 mm yr^{-1}, sedim. 179 m)*[a]						
896-23R-1	148-896A-23R-1W-1-6	392	213	Moderately altered basalt breccia	0	3	
896-29R-64	148-896A-29R-1W-64-69	450	271	Slightly altered basalt with red patches	0	2	MC
Site 504	*(Lat. 1.23; Lon. -83.73; Age 5.9 Ma; spreading rate 72 mm yr^{-1}, sedim. 274.5 m)*[b]						
504-80R-44	83-504B-80R-1W-44-46	910	636	Moderately altered basalt	1	1	MC
504-81R-39	83-504B-81R-1W-39-42	920	646	Moderately altered hyaloclastic breccia	No	Yes	MC
504-143R-138	111-504B-143R-1W-138-142	1361	1087	Slightly altered doleritic basalt	1	1	MC
504-147R-31	111-504B-147R-2W-31-35	1399	1125	Slightly altered doleritic basalt	1	1	MC
504-147R-52	111-504B-147R-2W-52-55	1399	1125	Slightly altered doleritic basalt	1	1	MC
504-214R-112	140-504B-214R-1W-112-114	1820	1546	Moderately altered doleritic basalt	3	0	MC
504-251R-62	148-504B-251R-1W-62-65	2091	1817	Moderately altered dolerite	1	0	MC
Site 1256	*(Lat. 6.74; Lon. -91.93; Age 15 Ma; spreading rate 210 mm yr^{-1}, sedim. 250.7 m)*[c]						
1256-12R-11	206-1256C-12R-3W-11-17	316	66	Moderately altered basalt	0	2	MC
1256-61R-131	206-1256D-61R-1W-131-135	679	429	Moderately altered basalt	0	2	
1256-170R-21	309-1256D-170R-1W-21-25	1252	1002	Moderately altered doleritic basalt	1	0	MC
1256-170R-63	309-1256D-170R-3W-63-66	1255	1005	Moderately altered doleritic basalt	0	0	MC
1256-174R-99	312-1256D-174R-1W-99-109	1266	1016	Completely altered basalt	Yes	No	
1256-214R-95	312-1256D-214R-1W-95-98	1412	1162	Heavily altered gabbro	3	0	
1256-227R-142	312-1256D-227R-1W-142-143	1470	1220	Recrystallized dolerite	3	0	MC
Site 1149	*(Lat. 32.00; Lon. 146.00; Age 132 Ma; spreading rate 102 mm yr^{-1}, sedim. 307 m)*[d]						
1149-8R-119	185-1149D-8R-1W-119-124	330	23	Slightly altered basalt	0	2	TC+TH
1149-9R-57	185-1149D-9R-3W-57-64	342	35	Moderately altered basalt	0	3	TH
Site 801	*(Lat. 18.64; Lon. 156.36; Age 170 Ma; spreading rate 160 mm yr^{-1}, sedim. 493.7 m)*[e]						
801-10R-74	129-801C-10R-3W-74-81	573	79	Slightly altered dolerite	0	2	TH
801-15R-47	185-801C-15R-3W-47-50	617	123	Moderately altered basalt	0	2	TH
801-16R-115	185-801C-16R-1W-115-120	624	130	Moderately altered doleritic basalt	0	3	TH
801-19R-47	185-801C-19R-2W-47-51	654	160	Moderately altered basalt	0	2	TH
801-19R-58	185-801C-19R-3W-58-61	655	161	Moderately altered basalt	No	Yes	TC+TH
801-21R-111	185-801C-21R-2W-111-116	673	179	Moderately altered doleritic basalt	0	2	TH
801-31R-46	185-801C-31R-4W-46-51	761	267	Slightly altered doleritic basalt	0	2	TC+TH
801-44R-62	185-801C-44R-2W-62-64	881	387	Moderately altered dolerite	0	3	TH
801-45R-25	185-801C-45R-1W-25-30	889	395	Moderately altered basalt	0	2	TH
801-45R-90	185-801C-45R-1W-90-94	889	395	Slightly altered basalt	0	3	TH

Sample abbrev. name = sample abbreviated name as appearing in this article, sample full name = sample name as found in IODP reports, named as follows: leg-site-hole-core-section-interval (top–bottom in cm), mbsf = metres below seafloor, msb = metres sub-basement, main 2nd mineral. = main secondary mineralogy, amph. = amphibole, mineral proportion compared to the whole mineralogy: 0 = 0%; 1 = <5%; 2 = 5–20%; 3 = 20–50%; 4 = > 50%, if the proportion could not be quantified, due to the highly heterogeneous alteration of the sample, yes and no indicate respectively the presence or absence of a mineral. Lat. = latitude, Lon. = longitude, sedim. = sediments thickness overlying basement, the references provide information on each site.
All the samples have been analysed for halogens by crushing and heating using the MS1 mass spectrometer, following the irradiation method. The method and location for noble gas isotopes and abundances measurements are indicated in the column NG (noble gas) isotopes analysis: MC = crushing at the University of Manchester; TC = crushing at the University of Tokyo; TH = heating at the University of Tokyo.

[a] Alt et al. (1993).
[b] Anderson et al. (1985) (leg 83), Becker et al. (1988) (leg 111), Dick et al. (1992) (leg 140), Alt et al. (1993) (leg 148).
[c] Wilson et al. (2003) (leg 206), Teagle et al. (2006) (legs 309/312).
[d] Plank et al. (2000).
[e] Lancelot et al. (1990) (leg 129), Plank et al. (2000) (leg 185).

2011). We selected 28 samples of oceanic crust obtained by drilling in the Pacific Ocean at Ocean Drilling Program (DSDP and ODP) Sites 504, 801, 896, 1149 and 1256 (Fig. 1 and Table 1) that span an age range between 6 and 170 Ma. They were sampled from a depth range of 316–2091 m below sea floor (mbsf) or 23–1817 m sub-basement (msb) in altered oceanic crust (Table 1). The samples include 21 basalts, 4 dolerites, one basalt breccia, one hyaloclastite breccia and one gabbro.

2.1. Geological background

Among the 28 samples, 16 are from relatively young oceanic crust, in the eastern Pacific Ocean (Sites 504, 896

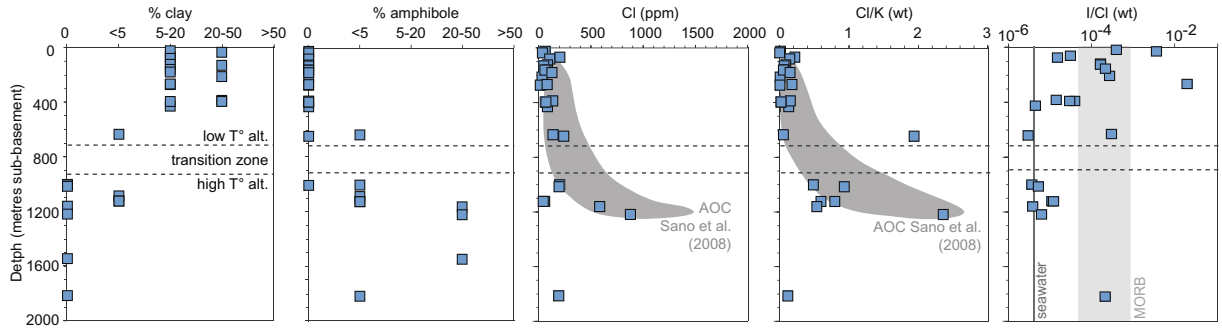

Fig. 2. Relationship between the depth and the mineralogy of the samples (% clays and % amphibole) and Cl, Cl/K and I/Cl. The dotted line represents the transition from volcanic lavas to intrusive sheeted dikes for sites 504 and 1256 (Alt et al., 1989, 2010).

and 1256) and 12 are from the western Pacific Ocean, where the crust is older (Sites 801 and 1149).

Sites 504 and 896 are 1 km apart and located on young ocean crust (5.9 Ma), 201 km south of the easternmost segment of the Galapagos spreading centre on the Nazca plate, at the Costa Rica Rift (6.8 cm yr^{-1} full spreading rate). The 9 samples from these locations are from between 213 and 1817 msb. The shallowest sample is a basalt breccia and the two deepest samples are dolerites (1546 and 1817 msb, Alt et al., 1993).

ODP Site 1256 is located in the Guatemala Basin on the Cocos plate in the eastern Pacific Ocean. The ocean crust formed at a superfast spreading rate ~15 Ma ago (20–22 cm yr^{-1}) on the East Pacific Rise (Wilson et al., 2003; Teagle et al., 2006). Samples from this site comprise 6 altered basalts and dolerites and 1 gabbro. They span a large range of depths between 66 and 1220 msb. Alteration in Hole 1256D is described by Alt et al. (2010).

Site 1149 is in 132 Ma old oceanic crust and sediments that are being transported into the Izu-Bonin subduction zone. The 2 altered basalts studied are from shallow depths (23 and 35 msb). Site 801 samples the oldest crust in the modern ocean and is a reference site for the Jurassic oceanic crust (170 Ma) and overlying sediments that are being subducted into the Mariana Trench. The 10 altered basalts and dolerites from this site come from relatively shallow depths (from 79 to 395 msb).

2.2. Sample description

Thin section observations show that the samples are heterogeneous down to the microscopic scale. They contain hydrothermal veins of different compositions, sizes and quantity (Supplementary Material Table A). Fluid inclusions are present in veins and minerals of the groundmass (petrographic details of typical thin sections are shown in the Fig. A of the Supplementary Material). Basalts are characterised by aphyric textures with very fine-grained matrices. Plagioclase microlites are typically 20–200 μm sized. Doleritic basalts and dolerites contain intermingled crystals of different sizes, from the micron to millimeter scale. To determine the mineral phase modality, we performed XRD measurements and optical microscopy. The XRD determination utilised a Bruker D8 Advance X-ray diffractometer with CuKα_1 radiation at 40 kV and 40 mA. The main primary minerals identified are plagioclase feldspar and clinopyroxene. However, variations in XRD spectral peak heights in different aliquots of the same sample indicated different proportions of these minerals suggesting significant heterogeneity. There was considerable noise in the XRD spectra due to the heterogeneity of the samples. We therefore combined the XRD results with a visual assessment of the thin sections using optical microscopy to determine the main mineral modes using intervals: 0%, <5%, 20–50% and >50% (Table 1 and Supplementary Material Table A).

Primary minerals show different degrees of alteration and are either intact, partially or fully replaced by secondary minerals. Olivine is almost completely altered, and most commonly replaced by clay minerals. The main secondary phases are chlorite, amphibole and Mg-saponite clay. Other secondary phases present in minor amounts include celadonite, goethite, pyrite, quartz, zeolite, carbonate, epidote, prehnite and talc. Opaque minerals are ubiquitous and are generally oxides such as magnetites and titanomagnetites. Alteration veins (~80 μm–1 mm) are present in some samples, comprised mostly of quartz, iron-oxyhydroxides and clay saponite (Supplementary Material Table A).

There is a major change in primary textures and secondary mineralogy in the transition located at 800–900 msb, from erupted lavas to basalts intruded into the sheeted dike complex. Low temperature alteration minerals such as clays are present above 800–900 msb, whereas high temperature alteration minerals such as amphiboles characterise deeper samples (Fig. 2). This change reflects the transition from fine-grained to aphyric volcanic lavas to intrusive sheeted dikes and plutonic rocks with a granular texture and a step increase in hydrothermal alteration temperature. This is in agreement with previous studies of AOC samples from a range of depths for sites 504 and 1256 (Alt et al., 1989, 2010). At Site 1256, the effects of alteration temperature are also reflected in oxygen isotope variations (Gao et al., 2012), with $\delta^{18}O$ values being higher in the extrusive basalts above 800–900 msb due to isotope exchange with seawater at temperatures below 200–250 °C.

Fluid inclusions are present in the thin sections studied here and in previous studies (e.g. Alt et al., 2010). The fluid

inclusions are typically ~1 μm in size and are principally observed in plagioclase and quartz composing the groundmass and, to a lesser extent, in clinopyroxene. We do not exclude the possibility that some fluid inclusions may be present in other mineral phases. It is not straightforward to investigate fluid inclusions in the shallower samples due to their aphyric or microlitic texture. Nevertheless, occasional inclusions have been identified in some plagioclase grains in these samples. Fluid inclusions are most easily visible in the deeper samples in which they can occur as individual fluid inclusions or as trails. Fluid inclusions appear to be more numerous in the deeper, high alteration temperature samples than in the shallower low alteration temperature samples. Where visible, the fluid inclusions are highly variable, and within a sample, they can consist of a single or two phases. In some of the largest fluid inclusions (up to 10 μm), the presence of a moving vapour bubble (less than ~10% the size of the fluid inclusion), indicates that they comprise mostly of a liquid phase. Some of the fluid inclusions contain daughter minerals, but these are too small to be identified.

Gaseous vesicles, found in fresh basalt glass, have not been preserved in the samples. In the deeper samples, relics of primary vesicles are not observed. In shallower samples, they are completely filled with secondary minerals, including clays (saponite), carbonates, celadonite and oxides.

3. ANALYTICAL TECHNIQUES

Noble gas isotope and abundance and halogen abundance determinations were carried-out using noble gas mass spectrometry. In order to extract noble gases and halogen-derived noble gases trapped in different sample phases, we used two extraction techniques. In vacuo stepped crushing was used to release gases from fluid or gas inclusions and/or from grain boundaries. In vacuo stepped heating was used to release the volatiles trapped in minerals, the matrices or other solid phases. Noble gas isotopic ratios in non-irradiated samples were analysed by crushing using an upgraded VG5400 mass spectrometer at the University of Manchester ($n = 12$ samples), by crushing at the University of Tokyo ($n = 3$) or by step heating only at the University of Tokyo ($n = 12$). Aliquots of each sample ($n = 28$) were neutron-irradiated to convert Cl, Br and I isotopes to Ar, Kr and Xe isotopes respectively. Halogen abundances were determined by crushing and then by heating of irradiated samples using the MS1 mass spectrometer in Manchester. The mineralogy of the samples was determined by XRD and optical microscopy (Section 2.2).

3.1. Selected fractions of samples

For each sample, a whole rock fraction comprising 0.5–2 mm sized chips was selected under the binocular microscope to be comparable with the material chips selected for the XRD measurements. We chose fragments which looked similar and which were the most representative of the sample and free of superficial alteration and weathering (See an example in the Supplementary Material Fig. B). Where possible, veins were avoided in order to analyse the groundmass content of the samples (Supplementary Material Fig. B). However, this was not possible where fine-scale μm-thick veins were present that could not be distinguished under a binocular microscope. The samples were too fined-grained to enable mineral separation thus whole-rock samples were used throughout for noble gas and halogen analyses (See example in the Supplementary Material Fig. A).

3.2. Noble gas isotopes and abundances in Manchester

Noble gas (^{4}He, ^{20}Ne, ^{40}Ar, ^{84}Kr, and ^{130}Xe) abundances and isotopic compositions (^{3}He/^{4}He, ^{20}Ne/^{22}Ne, ^{40}Ar/^{36}Ar, ^{86}Kr/^{84}Kr and ^{132}Xe/^{130}Xe) were obtained for twelve samples by crushing release. They were analysed using a VG5400 noble gas mass spectrometer, with upgraded electronics in order to improve instrument stability during measurements. About 0.5 g of mm-sized rock fragments were handpicked under a binocular microscope (Section 3.1). They were then washed in acetone followed by de-ionised water in an ultrasonic bath. After drying under a heat lamp, the samples were loaded into cylindrical stainless steel tube crushers (Sumino et al., 2001). They were baked under vacuum at ~150 °C over a 24 h period to reduce adsorbed atmospheric gases and were then left pumping for a further ~48 h to reach ultra-high vacuum (about 10^{-9} mbar). The samples were then mechanically crushed using an electromagnetic field to drive a nickel piston inside the tube crushers for a fixed number of cycles to form a 'crushing step'. For each sample, between 3 and 6 crushing steps were performed, each step corresponding to 100–3000 strokes (Supplementary Material Table B). After each crushing step, the noble gases were purified using a hot SAES GP50 getter for 10 min to remove active gases. The heavy noble gases Ar, Kr and Xe were then trapped on activated charcoal at 77 K (liquid nitrogen temperature). Helium and Ne were separated using a cryogenic trap at 45 K. After equilibration for 10 min the cryotrap was warmed to 57 K to fully release any trapped helium. Following helium isotope determination, the temperature was increased to 105 K to release Ne for isotopic analysis. Argon and then Kr and Xe were released from the charcoal cold finger and successively analysed in the mass spectrometer. At $m/z = 20$, $^{40}Ar^{++}$ and $^{20}Ne^{+}$ were partially resolved, enabling $^{40}Ar^{++}$, ($^{40}Ar^{++}$ + $^{20}Ne^{+}$) and $^{20}Ne^{+}$ to be measured. Resolution of $^{44}CO_2^{++}$ and $^{22}Ne^{+}$ at $m/z = 22$ is not possible in the VG5400 mass spectrometer and a correction factor was therefore required for $^{22}Ne^{+}$ determinations. The contribution from $^{44}CO_2^{++}$ at $m/z = 22$ was determined from the CO_2^{+} measurement at $m/z = 44$ and the CO_2^{++}/CO_2^{+} ratio. The CO_2^{++}/CO_2^{+} ratio was linearly inversely correlated with the amount of $^{20}Ne^{+}$ and $^{4}He^{+}$ and the correction line was determined after multiple air calibration analyses at varying $^{20}Ne^{+}$ and $^{4}He^{+}$ partial pressures. The typical CO_2^{++}/CO_2^{+} for the samples was 0.0066 ± 0.0008 (1σ, $n = 73$). Other background masses (CO_2 and H_2O) were monitored and CO_2^{++}/CO_2^{+} showed no significant variation within the observed range. Using corrections based on this calibration procedure, the $^{20}Ne/^{22}Ne$ ratios measured in air calibration

runs during the sample measurement period were 9.83 ± 0.07 ($n = 31$). Blank measurements were run at the start of each day and average values represent 7%, 5%, 1% and 0.5% of ^{4}He, ^{20}Ne, ^{36}Ar and ^{84}Kr–^{130}Xe respectively released during a step release from a sample. Blanks ($n = 75$) were on average $0.037 \pm 0.006 \times 10^{-9}$ cm^3 STP ^{4}He, $0.017 \pm 0.001 \times 10^{-10}$ cm^3 STP ^{20}Ne, $0.018 \pm 0.003 \times 10^{-10}$ cm^3 STP ^{36}Ar, $0.0036 \pm 0.0004 \times 10^{-11}$ cm^3 STP ^{84}Kr, $0.0033 \pm 0.0005 \times 10^{-13}$ cm^3 STP ^{130}Xe. The higher proportions of blank for the light noble gases are due to the lower concentrations of these gases in the samples. Similarly, some ^{3}He/^{4}He ratios have large uncertainties, up to ± 2.5 R_A, due to the low ^{3}He and ^{4}He concentrations in the samples.

3.3. Noble gases isotopes and abundances in Tokyo

Abundances of major isotopes (^{4}He, ^{20}Ne, ^{40}Ar, ^{84}Kr, and ^{132}Xe) and isotopic ratios (^{3}He/^{4}He, ^{20}Ne/^{22}Ne, ^{21}Ne/^{22}Ne, ^{38}Ar/^{36}Ar, and ^{40}Ar/^{36}Ar) of noble gases were determined with a noble gas mass spectrometer MS-IV (modified VG5400) at the Geochemical Research Centre, University of Tokyo. Noble gases were extracted by step-heating in vacuum for twelve samples and crushing extraction in three samples. 0.5–2 mm-sized grains were washed in ethanol followed by de-ionised water in an ultrasonic bath. After drying the samples in an oven at about 120 °C, ca. 0.2 g of the samples were wrapped in Al foil 10 μm thick and loaded in a sample holder made of Pyrex glass connected to a vacuum line and a Ta resistance–irradiation extraction furnace. For the crushing experiments, about 0.5 g of the samples was loaded into the crushers (Sumino et al., 2001). Prior to sample analysis, the extraction and purification systems containing the samples were baked-out under vacuum at 150 °C for more than one day. Two or three heating steps were applied, heating at 400 °C for 60 min (twice for some samples) and 1700 °C for 30 min (Supplementary Material Table C). Single step crushing with 2000 strokes of the nickel piston were performed in each crushing extraction. Purification, separation, and isotope ratio analysis of evolved noble gases are described in Sumino et al. (2001). Sensitivities and mass discrimination factors for all noble gases, except He, were determined by repeated measurements of known amounts of atmospheric gas. The mass discrimination factor for He isotope ratios was calibrated by measurements of HESJ standard gas, with a ^{3}He/^{4}He ratio of $(28.88 \pm 0.14) \times 10^{-6}$ (Matsuda et al., 2002). Neon isotope ratios were corrected for interferences from $^{40}Ar^{++}$ and CO_2^{++} on $^{20}Ne^{+}$ and $^{22}Ne^{+}$, respectively. The $^{40}Ar^{++}/^{40}Ar^{+}$ and CO_2^{++}/CO_2^{+} ratios were determined following Osawa (2004). Other background masses (H_2, CH_4, and H_2O) were monitored and the $^{40}Ar^{++}/^{40}Ar^{+}$ and CO_2^{++}/CO_2^{+} ratios showed no significant variation within the observed range. Blank levels of ^{4}He, ^{20}Ne, ^{40}Ar, ^{84}Kr, and ^{132}Xe in the step-heating measurements were lower than 3×10^{-9}, 3×10^{-12}, 2×10^{-9}, 3×10^{-13}, and 5×10^{-14} cm^3 STP, and those in the crushing measurements were lower than 2×10^{-10}, 3×10^{-12}, 6×10^{-10}, 6×10^{-14}, and 6×10^{-15} cm^3 STP, respectively.

3.4. Halogens

Neutron irradiation of samples converts Cl, Br, I, K (and Ca, Ba and U) into noble gas isotopes and forms the basis of both Ar-Ar geochronology and neutron activated halogen/trace element determination in natural samples (Turner, 1965; Böhlke and Irwin, 1992; Johnson et al., 2000). The measurements of the noble gas proxies for halogen concentrations produced by neutron irradiation were carried-out using the MS1 mass spectrometer, using in vacuo step crushing followed by in vacuo step heating. The experimental protocol is the same as used previously by Sumino et al. (2010).

About 0.05 g of mm-sized grains of each sample free of superficial alteration was handpicked under a binocular microscope. Samples were then washed in acetone followed by de-ionised water in an ultrasonic bath. After being dried under a heat lamp they were wrapped in Al foil envelopes, packed in quartz vials, sealed under vacuum and sent for irradiation at the Petten reactor, the Netherlands. Each tube contained Hb3gr flux monitors ($t = 1073.6 \pm 4.6$ Ma; Jourdan et al., 2006) distributed at the bottom, middle and top of each vial to monitor the neutron fluxes. The Shallowater meteorite monitor (Turner, 1965) was used to determine the conversion of I to ^{128}Xe, and indirectly Br to ^{80}Kr. The samples were then loaded into modified Nupro® valve-crushers (Stuart et al., 1994) and baked at ~150 °C for 24 h prior to crushing. Between 1 and 6 crushing steps was performed for each sample. One crushing step consisted of between 1 and 25 strokes (Supplementary Material Table D). Following the crushing experiments, between 0.02 and 0.03 g of the residual powders were loaded into a resistance furnace for stepwise thermal release. Heating experiments consisted either of 3 steps at 600 °C, 1400 °C and 1600 °C or sometimes in 2 steps at 1400 °C and 1600 °C (Supplementary Material Table D).

The noble gas production ratios $^{37}Ar_{Ca}$/Ca, $^{38}Ar_{Cl}$/Cl and $^{39}Ar_K$/K were monitored using Hb3Gr flux monitors in order to determine the fast and thermal neutron fluxes. The production ratios $^{80}Kr_{Br}$/Br and $^{128}Xe_I$/I were monitored using pyroxene separates of the Shallowater meteorite following the method described in Johnson et al. (2000). The measured ^{128}Xe/^{129}Xe ratio of the irradiated Shallowater meteorite with a known ^{129}I/^{127}I ratio ($(1.125 \pm 0.012) \times 10^{-4}$, Hohenberg, 1967) is used to determine the resonant flux. The irradiation yielded the following parameters: a mean J value of 0.00719 ± 0.00023 (1σ), an α value (the production efficiency of $^{39}Ar_K/^{37}Ar_{Ca}$ to K/Ca) ranging from 0.4159 ± 0.0018 to 0.4953 ± 0.0008, a β value (the production efficiency of $^{39}Ar_K/^{38}Ar_{Cl}$ to K/Cl) ranging from 8.49 ± 0.07 to 9.67 ± 0.06, a fast neutron flux of $1.37 \pm 0.04 \times 10^{18}$ n cm^{-2}, a thermal neutron flux of $7.0 \pm 0.4 \times 10^{18}$ n cm^{-2} and a resonant neutron flux of $1.2 \pm 0.3 \times 10^{17}$ n cm^{-2}. The Ar isotope measurements were corrected for neutron interferences and converted to parent K, Cl concentrations using the irradiation parameters and previously determined compositions of the Hb3gr monitor (Roddick, 1983). External precision (2σ) is 1.2% and 1.4% for Cl and K, but is higher for Br because it has not been monitored directly and I because of uncertainties associated

with neutron absorption cross-sections. A conservative estimate of 5–8% uncertainty for Br and 15% for I is based on our comparison with data from scapolite standard (Kendrick, 2012a) obtained in subsequent irradiations. Detection limits are equivalent to 0.5×10^{-8} g for Cl and 10^{-13} g for Br and I. The blank value associated with the largest release step of a sample was on average 2% for ^{38}Ar, ^{80}Kr, and ^{128}Xe.

4. RESULTS

Noble gas and halogen data are presented in Tables 2 and 3 and Supplementary Material Tables B-C-D for the details of each crushing and heating step. In the following, elemental ratios of noble gas will be presented as molar ratios while halogens ratios will be presented as weight ratios. Associated errors are 1σ unless otherwise stated. Note that the crushing data are reported as concentrations for mass of sample. However crushing primarily releases gases from fluid inclusions and these represent probably much less than 1% vol of the sample, thus halogen and noble gas concentrations in the fluid phase are likely to be much greater than indicated by the data given in Tables 2 and 3.

4.1. Noble gases

The $^{3}He/^{4}He$ ratios of the samples obtained by crushing range from 0.5 to 9.6 R_A, with the higher values found in the younger samples (5.9–15 Ma old). The $^{40}Ar/^{36}Ar$ ratios of crushed samples are close to the atmospheric value (298.6) and lower than ~310, except for the 3 oldest samples with ratios up to ~670. The 132–170 Ma old samples analysed using step heating indicate $^{3}He/^{4}He$ ratios lower than 0.4 Ra and $^{40}Ar/^{36}Ar$ ratios up to 1800 (Table 2). ^{4}He concentrations obtained by crushing vary by more than two orders of magnitude, ranging from 0.91 ± 0.06 to $407 \pm 3 \times 10^{-9}$ cm^3 STP g^{-1} (Table 2). The samples analysed using step heating are characterised by higher ^{4}He contents ($^{4}He = 0.53$ to 2.14×10^{-6} cm^3 STP g^{-1}) (Table 2). ^{40}Ar concentrations of crushed samples range from 0.05 to 3.40×10^{-6} cm^3 STP g^{-1}. ^{40}Ar concentrations of heated samples range from 0.62 to 3.56×10^{-6} cm^3 STP g^{-1}.

The $^{20}Ne/^{22}Ne$ ratio in the samples is 9.74 ± 0.12. The ^{20}Ne concentrations released by crushing range from 0.3 to 33×10^{-10} cm^3 STP g^{-1} (Table 2) and those obtained by heating vary between 0.9 and 9.5×10^{-10} cm^3 STP g^{-1}. The noble gas isotopic ratios of the heaviest noble gases are indistinguishable from the atmospheric values ($^{86}Kr/^{84}Kr = 0.3064 \pm 0.0024$, $^{132}Xe/^{130}Xe = 6.63 \pm 0.12$) (Table 2). The concentrations of ^{36}Ar range between 5 and 110×10^{-10} cm^3 STP g^{-1} in the crushed samples and 7 and 70×10^{-10} cm^3 STP g^{-1} in the heated samples. The ^{84}Kr and ^{132}Xe values are respectively between 0.6 and 45×10^{-11} cm^3 STP g^{-1} and 0.1 and 19×10^{-11} cm^3 STP g^{-1}.

Three samples have been analysed for noble gases using both crushing and heating. The measurements show that the amount of noble gas released by crushing represents from 1% to 40% the total content released (obtained by the heating experiments) depending on the isotope. Thus, for these samples, it is unlikely that the noble gases are mainly hosted in fluid inclusions (analysed using crushing experiments).

Noble gas ratios and concentrations from this study are consistent with the ranges reported by Staudacher and Allègre (1988) on AOC basalts from Jurassic Atlantic crust from Holes 418A and 417D and mid-Paleocene Indian crust from Sites 214 and 216 (Fig. 3) as well as 11 Ma gabbros from the Indian ocean crust (Moreira et al., 2003). Data for altered ocean crust samples from this study and from Staudacher and Allègre (1988) form a mixing trend on a plot of $^{130}Xe/^{36}Ar$ versus $^{84}Kr/^{36}Ar$ (Fig. 4A) and versus $^{22}Ne/^{36}Ar$ (Fig. 4B) for both crushing and heating experiments.

4.2. Halogens

Crushing of samples yielded geometric mean values of $Cl = 4^{+19}_{-3}$ ppm, $Br = 20^{+93}_{-17}$ ppb and $I = 0.3^{+0.8}_{-0.2}$ ppb, based on the log-normal distributions of their halogen concentrations (see Supplementary Material Fig. C for details about the mean calculations related to log-normal distributions). Stepped heating of the crushed residues gave geometric mean halogen concentrations of $Cl = 94^{+133}_{-55}$ ppm, $Br = 152^{+271}_{-97}$ ppb and $I = 3.6^{+19.2}_{-3.0}$ ppb (Supplementary Material Table D). On average, about 90% of the halogens are released during stepped heating. However, the deeper samples released significantly more Cl, Br and I by crushing than the shallower samples (~5% and 20% respectively). Deeper samples contain more fluid inclusions than the shallower samples, therefore the crushing releases are likely to be related to the halogen content of the fluid inclusions. Bulk rock contents, calculated by combining crushing and stepped heating measurements, range from 11 to 875 ppm for Cl, 44 to 2500 ppb for Br and 0.4 to 250 ppb for I (Table 3). The Cl contents are indistinguishable from the range of axial Pacific MORB (obtained from the PETDB database, Lehnert et al., 2000, Fig. 5A). The K/Cl ratios of the samples range from 0.4 to 148 (Fig. 5A) within the range of axial Pacific whole rock MORB of between 0.5 and 170 ($n = 220$, compilation from PETDB, Lehnert et al., 2000). Fig. 5B shows a linear positive correlation ($r^2 = 0.96$) between Br and Cl, with a mean ratio $Br/Cl = 2.0 \pm 1.1 \times 10^{-3}$. The Br/Cl ratios are similar to or lower than the seawater Br/Cl ratio (3.5×10^{-3}) and the MORB Br/Cl ratios ($2.6 \pm 0.7 \times 10^{-3}$, 1σ, $n = 71$, using the data of Schilling et al. (1980) Jambon et al. (1995) and Kendrick et al. (2012b) revised downwards in Kendrick et al. (2013a)). In our study, half of the samples have a ratio lower than 2.0×10^{-3} (i.e. below the 1σ standard deviation limit of the MORB average). In contrast, crushing results yielded Br/Cl values higher than that obtained during heating and with one exception, all are higher than the seawater Br/Cl value (Fig. 6). Fig. 5C shows I/Cl ratios of the whole rocks varying by up to 4 orders of magnitude for similar Cl contents. The I/Cl values obtained by crushing and by heating are similar (Fig. 6). The halogen compositions in the oceanic crust show a change at a depth

Table 2
Noble gas abundances and isotopic compositions obtained on unirradiated samples.

Sample cc/g STP	Weight (g)	Steps str. #	^{4}He (10^{-9})	±	^{20}Ne (10^{-10})	±	^{36}Ar (10^{-10})	±	^{84}Kr (10^{-11})	±	^{130}Xe (10^{-13})	±	^{132}Xe (10^{-11})		R/R_A	±	^{20}Ne/^{22}Ne	±	^{40}Ar/^{36}Ar	±	^{86}Kr/^{84}Kr	±	^{132}Xe/^{130}Xe	±
Crushing																								
504-80R-44	0.4762	2600	0.91	0.06	5.96	0.07	22.73	0.13	7.39	0.20	8.53	0.39			[*]-	-	9.92	0.17	297.8	2.3	0.303	0.012	6.59	0.39
504-81R-39	0.6020	5100	1.34	0.12	13.67	0.29	78.97	0.27	28.99	0.93	33.46	0.70			7.2	3.4	9.80	0.29	298.4	1.2	0.308	0.014	6.42	0.18
504-143R-138	0.4414	2600	3.28	0.05	6.99	0.07	31.00	0.10	11.12	0.17	14.30	0.25			8.4	2.0	9.80	0.15	298.9	1.2	0.307	0.007	6.71	0.14
504-147R-31	0.5188	1600	2.31	0.03	-	-	6.65	0.05	2.89	0.20	5.08	0.14			9.2	2.1	-	-	298.7	2.4	0.305	0.030	6.80	0.22
504-147R-52	0.4057	8100	7.14	0.07	4.48	0.10	23.59	0.13	8.95	0.20	19.91	1.04			6.7	1.5	9.60	0.32	299.5	2.3	0.309	0.010	6.65	0.43
504-147R-52	0.4177	5100	5.65	0.06	-	-	26.36	0.18	10.03	0.28	20.01	1.28			6.8	1.6	-	-	300.4	2.8	0.306	0.012	6.70	0.54
504-147R-52	0.3623	5100	5.08	0.06	3.34	0.10	19.46	0.13	8.40	0.21	20.00	1.23			5.9	2.0	9.39	0.39	303.0	2.9	0.306	0.011	6.54	0.50
504-147R-52	mean		5.95	0.11	3.91	0.14	23.14	0.26	9.13	0.41	19.98	2.06			6.5	2.9	9.50	0.50	301.0	4.6	0.307	0.019	6.63	0.86
504-214R-112	0.4740	2600	9.46	0.07	5.80	0.06	19.83	0.07	7.49	0.48	11.56	0.29			6.9	1.0	9.85	0.15	299.9	1.3	0.305	0.028	6.46	0.19
504-251R-62	0.5106	4100	22.78	0.13	3.65	0.03	20.31	0.06	8.75	0.33	14.96	0.29			6.2	0.5	9.63	0.15	298.3	1.1	0.306	0.017	6.85	0.15
896-29R-64	0.5564	3600	1.12	0.04	0.75	0.01	8.21	0.06	3.39	0.09	7.60	0.34			9.6	4.2	9.63	0.27	308.1	2.6	0.305	0.012	6.67	0.39
1256-170R-21	0.3931	9100	332.85	0.57	33.42	0.71	110.81	0.54	34.72	0.81	49.01	2.46			6.7	0.2	9.81	0.29	306.4	2.1	0.307	0.010	6.57	0.42
1256-170R-63	0.4998	2600	73.85	0.39	6.81	0.08	54.00	0.29	21.19	0.57	29.66	1.31			5.6	0.2	9.81	0.16	305.4	2.3	0.306	0.012	6.64	0.39
1256-227R-142	0.5796	2600	407.02	2.51	5.80	0.08	12.83	0.09	4.31	0.14	5.36	0.28			5.6	0.2	9.91	0.20	312.4	2.9	0.304	0.014	6.61	0.45
1256-12R-11	0.4542	4100	29.07	0.16	3.84	0.03	101.42	0.25	85.90	5.01	290.21	6.17			4.2	0.5	9.64	0.15	300.6	1.0	0.313	0.026	6.66	0.17
1149-8R-119	0.5300	2000	6.18	0.33	0.41	0.07	2.59	0.15	1.02	0.11			0.08	0.01	0.9	0.3	9.80	0.09	675.3	17.9				
801-19R-58	0.5106	2000	7.41	0.37	0.25	0.04	5.30	0.27	9.52	0.95			2.78	0.28	0.5	0.3	9.82	0.10	330.2	0.3				
801-31R-46	0.5257	2000	83.9	4.2	0.68	0.07	1.57	0.08	0.62	0.06			0.09	0.01	3.7	0.1	9.84	0.08	338.4	0.5				
Heating																								
1149-8R-119	0.2240	Total	805	32	9.47	1.20	68.17	3.12	44.94	4.02			13.38	1.17	0.001	0.013	9.81	0.11	425	3				
1149-9R-57	0.2990	Total	967	47	0.87	0.13	41.54	2.03	13.05	0.93			1.22	0.09	0.243	0.028	9.73	0.12	857	8				
801-10R-74	0.2452	Total	993	9	2.86	0.93	25.99	2.39	15.20	1.40			3.34	0.04	0.133	0.012	9.66	0.22	357	4				
801-15R-47	0.2086	Total	597	28	2.68	0.21	15.25	0.55	3.83	0.28			0.49	0.04	0.304	0.014	9.75	0.03	590	3				
801-16R-115	0.1966	Total	535	26	1.80	0.20	12.34	0.46	10.75	0.79			1.78	0.13	0.382	0.049	9.76	0.08	543	6				
801-19R-47	0.1958	Total	2143	103	2.57	0.20	13.26	0.49	6.63	0.54			1.42	0.13	0.025	0.003	9.70	0.05	1002	6				
801-19R-58	0.2160	Total	1201	56	1.78	0.14	25.47	0.98	34.50	3.00			16.34	1.46	0.021	0.003	9.78	0.05	581	1				
801-21R-111	0.2124	Total	1146	12	1.90	1.10	12.85	0.91	7.20	0.68			1.42	0.02	0.129	0.011	9.86	0.42	483	23				
801-31R-46	0.2006	Total	947	33	1.70	0.14	6.79	0.32	3.02	0.27			0.53	0.05	0.275	0.008	9.73	0.05	1024	13				
801-44R-62	0.2190	Total	757	27	2.00	1.00	31.47	1.54	25.90	2.41			11.64	1.07	0.146	0.092	9.64	0.46	371	4				
801-45R-25	0.2146	Total	946	45	3.69	0.29	12.95	0.51	5.08	0.38			0.78	0.06	0.039	0.004	9.77	0.05	1644	11				
801-45R-90	0.1972	Total	741	29	3.84	0.28	12.61	0.51	5.31	0.46			0.74	0.06	0.069	0.006	9.80	0.05	1804	15				

Concentrations are given in cm^3 STP g^{-1}, blank data are in cm^3 STP.

[*] ^{3}He below detection. The details of each step are provided in Supplementary Material Tables B and C.

Table 3
Halogen total releases obtained on irradiated samples.

Sample	K ppm	±	Cl ppm	±	Br ppb	±	I ppb	±
Altered MORB								
896-23R-1	2315	134	30	2	85.8	12.3	7.5	2.0
896-29R-64 a	1535	81	11	1	24.0	3.6	478.3	136.8
896-29R-64 b	960	50	16	1	93.3	15.3	22.4	6.1
896-29R-64 mean	1248	407	14	3	58.7	49.0	250.3	322.4
504-80R-44	2225	395	135	17	392.9	24.2	37.9	10.2
504-81R-39	123	4	237	9	785.0	20.7	0.7	0.1
504-143R-138								
504-147R-31	92	5	55	3	144.2	18.7	0.59	0.1
504-147R-52	52	6	41	1	123.8	4.3	0.5	0.1
504-214R-112					814.9	43.9	1.5	0.2
504-251R-62	1545	131	191	12	643.2	34.6	37.9	9.2
1256-12R-11	895	27	200	5	373.3	19.8	5.9	1.0
1256-170R-21	405	30	198	13	460.1	47.7	0.7	0.1
1256-170R-63					340.7	20.1	1.7	0.3
1256-174R-99 part 1	81	6	126	3	297.5	18.6	1.0	0.1
1256-174R-99 part 2	37	5	106	2	86.5	4.1	0.7	0.1
1256-174R-99 part 3	503	19	346	18	696.2	35.5	1.2	0.1
1256-174R-99 mean	207	257	193	133	360.1	309.6	1.0	0.3
1256-214R-95	1080	19	582	13	1490.3	152.8	2.1	0.3
1256-227R-142	373	9	875	14	2484.4	80.3	5.2	0.4
1256-61R-131	601	42	82	7	82.0	15.0	0.4	0.1
1149-8R-119	3233	38	60	1	56.4	1.9	21.9	2.4
1149-9R-57	4706	33	34	1	71.8	0.7	113.4	1.6
801-10R-74	685	10	103	2	87.3	3.0	1.5	0.2
801-15R-47	868	15	81	3	234.7	2.0	12.6	0.4
801-16R-115	652	11	46	1	44.3	0.3	7.1	0.4
801-19R-47	941	18	77	2	69.7	0.5	15.7	0.4
801-19R-58	973	7	58	1	86.5	1.1		
801-21R-111	809	11	125	8				
801-31R-46	431	8	79	2	97.6	1.0		
801-44R-62	824	12	132	9	98.0	14.4	1.8	0.2
801-45R-25	2448	18	62	1	58.9	0.5	2.3	0.5
801-45R-90	2667	17	66	2	73.8	1.4	1.9	0.2

The details of each step crushing and heating are provided in Supplementary Material Table D.

of ~800–900 msb (Fig. 2). Chlorine and Br concentrations are higher below this depth, whereas I is lower. At depths shallower than 800–900 msb, the Cl/K is lower than MORB and the log mean I/Cl ratio is $\sim 10^{-4}$, similar to MORB values. At deeper levels (>800–900 msb), Cl/K is higher and I/Cl is lower ($\sim 10^{-5}$).

5. DISCUSSION

Using our new halogen and noble gas data of AOC samples as representative of the ocean crust we consider possible carrier phases to address the following questions. Do the same phases host both halogens and noble gases? What is the source (e.g. seawater, brines) of these elements? Is there any fractionation prior to the subduction process? Knowledge of the processes that fix the noble gases and halogens in the altered oceanic crust will allow a quantitative understanding to be developed, as well as an appreciation for the spatial/depth control on the abundance and character of halogen/noble gases in the altered oceanic crust prior to subduction.

5.1. Intra- and inter-sample variability

Crushing three visually similar aliquots of sample 504-147R-52 yielded a reproducibility (intra-sample variability) of better than 20% for all noble gas abundances (1σ) (Table 2). Between the samples, the variation ranges from 100% to 200% (inter-sample variability). For the halogens, analyses of multiple fractions of the same sample show that high halogen heterogeneity can exist within a sample (Table 3). For example, in the two analysed fractions of sample 896-29R-64, although the Cl measurements are relatively reproducible ±20% (1σ), the Br and I releases show a variation of ~100%. In sample 1256-174R-99, the three different fractions analysed are variable by 70%, 90% and 30% for Cl, Br and I respectively. In comparison, the variability (1σ) between the different samples averages 130%, 150% and 250% for Cl, Br and I respectively (Table 3). Despite the fact that the halogens can be variable within a sample, the observed variation between the samples is much greater, allowing for meaningful comparisons between them to be made.

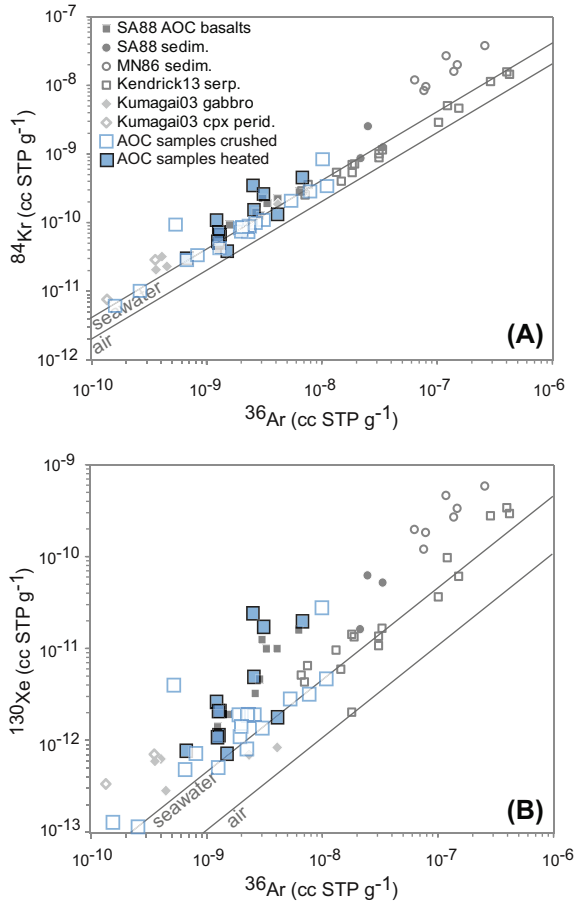

Fig. 3. Heavy noble gas elemental concentrations. (A) ^{84}Kr versus ^{36}Ar and (B) ^{130}Xe versus ^{36}Ar; sedim. = sediments, serp. = seafloor serpentines, cpx perid. = clinopyroxene peridotite. SA88 = Staudacher and Allègre (1988), MN86 = Matsuda and Nagao (1986), Kendrick13 = Kendrick et al. (2013b), Kumagai03 = Kumagai et al. (2003).

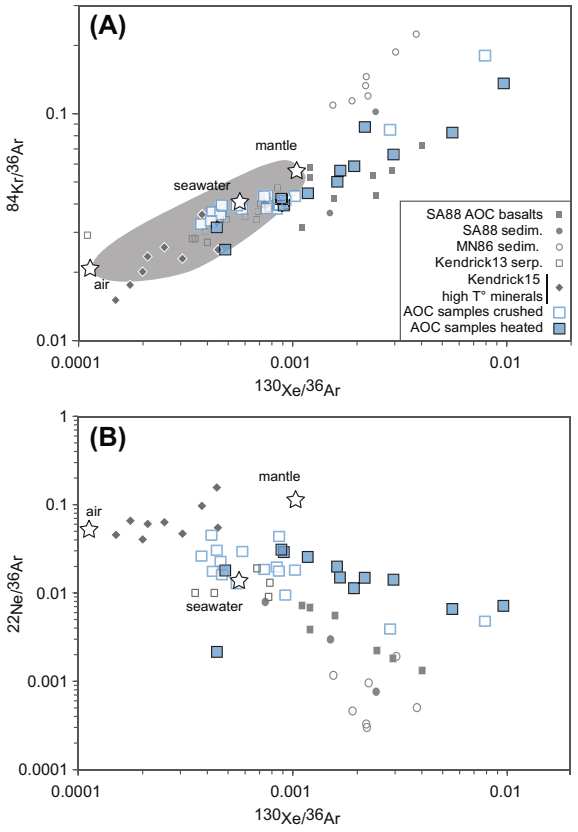

Fig. 4. Noble gas mixing diagrams. (A) $^{84}Kr/^{36}Ar$ versus $^{130}Xe/^{36}Ar$ and (B) $^{22}Ne/^{36}Ar$ versus $^{130}Xe/^{36}Ar$. SA88 = Staudacher and Allègre (1988), SA88 sedim. = sediments of Staudacher and Allègre (1988), MN86 sedim. = sediments of Matsuda and Nagao (1986), Kendrick13 serp. = oceanic serpentinites of Kendrick et al. (2013b), Kendrick15 high T minerals = amphibole, quartz and epidotes from oceanic metagabbros (Kendrick et al., 2015), mantle composition derived from CO_2 well gases data (Holland and Ballentine, 2006), popping-rock (Burnard et al., 1997; Moreira et al., 1998) (see Ballentine et al. (2005) and Holland and Ballentine (2006) for explanations of the mantle composition), grey field: MORB from PETDB database (Lehnert et al., 2000), in B) $^{22}Ne/^{36}Ar$ ratios from the literature are calculated using the $^{20}Ne/^{36}Ar$ ratios in Kendrick13, SA88 and MN86 considering an atmospheric $^{20}Ne/^{22}Ne$ ratio of 9.8.

5.2. Origin of the halogen and noble gases signature

5.2.1. Overprinting of the isotopic noble gas primary signature and radiogenic noble gases

Apart from $^{3}He/^{4}He$ ratios and some of the $^{40}Ar/^{36}Ar$ ratios, the isotopic ratios of other noble gases are close to atmospheric values. This indicates that the primary mantle signature has been overprinted by air or seawater. Our data also show no evidence for isotopic fractionation effects resulting from adsorption (Marrocchi et al., 2011) associated with alteration processes, as has been previously suggested for Xe in sediments (Podosek et al., 1981; Matsuda and Nagao, 1986).

The $^{3}He/^{4}He$ and $^{40}Ar/^{36}Ar$ ratios of the samples can be divided in two groups based upon age: the younger samples (5.9–15 Ma) and the older samples (132–170 Ma). The average $^{3}He/^{4}He$ ratio of the 5.9–15 Ma old samples (Sites 504, 896, 1256) released by crushing is 6.9 ± 1.6 R_A. This is similar to the recently reviewed MORB average of 8.0 ± 1.5 R_A (Sano and Fischer, 2013). It suggests that a mantle helium component is still preserved in these samples. Since gaseous vesicles have not been preserved in the samples, or are filled with secondary minerals (Section 2.2), the source of the magmatic ^{3}He is more likely fluid inclusions. It also indicates that almost no radiogenic ^{4}He is present, in agreement with the $^{40}Ar/^{36}Ar$ ratios ($^{40}Ar/^{36}Ar = 302.2 \pm 4.8$) close to the air value indicating no in-situ K-derived ^{40}Ar in the fluid inclusions (=crushing data). In contrast, the crushing releases of the older samples (Sites 801, 1149) are characterised by lower $^{3}He/^{4}He$ (0.5–3.7 R_A) and higher $^{40}Ar/^{36}Ar$ ratios (330–675) indicating the presence of radiogenic ^{4}He and ^{40}Ar. This is supported by results from the same age samples analysed using heating, yielding $^{3}He/^{4}He < 0.4$ R_A and $^{40}Ar/^{36}Ar$ ratios up to 1800. These values result from the release of radiogenic U- and Th- derived ^{4}He and K-derived ^{40}Ar from the minerals during heating. However, based upon typical concentrations of U, Th

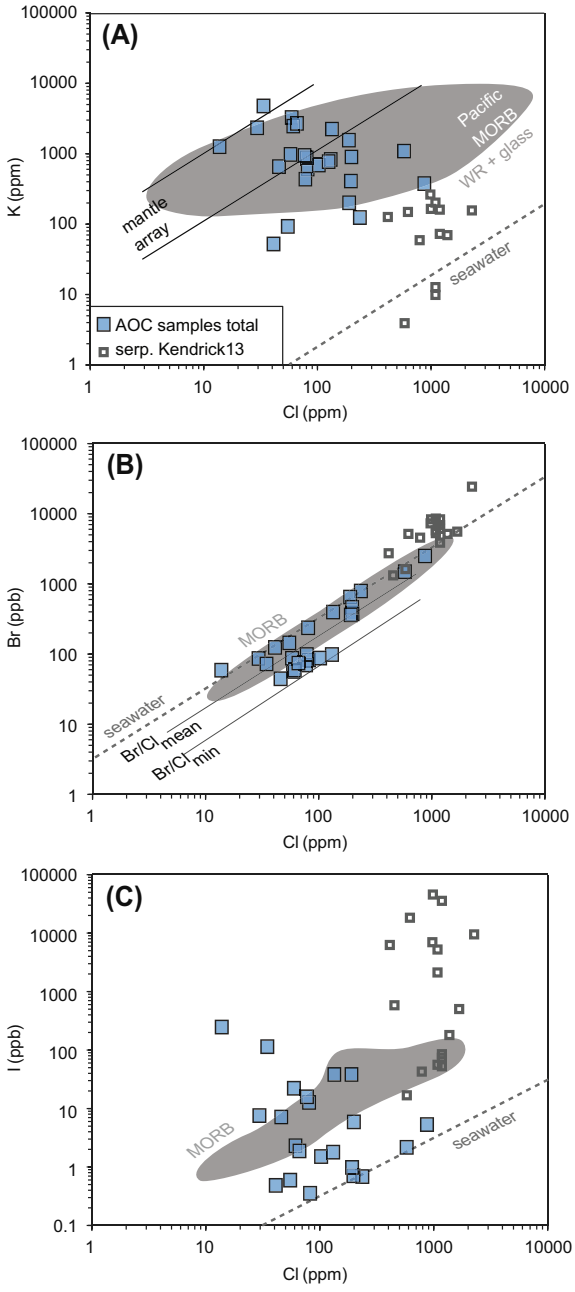

Fig. 5. Halogen abundances in AOC samples. (A) K versus Cl, (B) Cl versus Br and (C) Cl versus I. MORB field in (A) from the PETDB database (Lehnert et al., 2000), in (B) and (C) from Déruelle et al. (1992), Jambon et al. (1995), data of Kendrick et al. (2012b) revised downward in Kendrick et al. (2013a). The MORB dataset includes all data analysed on on-axis MORB, thus also comprising samples which have been affected by assimilation of a seawater derived component in the magma chamber or during the eruption (e.g. Michael and Cornell, 1998; Kendrick et al., 2013a), serp. Kendrick13 = oceanic serpentinites of Kendrick et al. (2013b).

and K present in AOC samples (Kelley et al., 2003) and the age of the samples, the levels of radiogenic ^{4}He and ^{40}Ar are lower than expected suggesting some loss has occurred during alteration (Staudacher and Allègre, 1988). Using the K contents of the samples obtained in this study and the K-Ar age, we estimate that ~50% of the ^{40}Ar radiogenic is missing. On average, younger samples contain more ^{36}Ar than older samples, also consistent with higher noble gas loss in older samples.

5.2.2. Hydrothermal alteration

Data obtained by crushing and heating samples are shown on plots of ^{84}Kr/^{36}Ar versus ^{130}Xe/^{36}Ar (Fig. 4A) and ^{22}Ne/^{36}Ar versus ^{130}Xe/^{36}Ar (Fig. 4B), also included are previous measurements of AOC samples. We note that the ^{22}Ne/^{36}Ar ratios of samples studied here are close to the seawater value in this study, and higher than literature data. The reason for this remains unclear. Several processes could account for the observed linear relationships shown in Fig. 4. It could represent two components mixing or result from noble gas fractionation during alteration or formation of secondary minerals. A mantle component is excluded because all the Kr and Xe isotopic ratios are air-like (Table 2). Some samples have ^{84}Kr/^{36}Ar and ^{130}Xe/^{36}Ar values which cluster close to the seawater composition (Fig. 4A), indicating that they are dominated by seawater-derived noble gases. ^{84}Kr/^{36}Ar and ^{130}Xe/^{36}Ar ratios lower than the seawater values suggest the presence of a modern air component, possibly acquired during recovery and preparation of the samples in the laboratory (e.g. Ballentine and Barfod, 2000). Higher ^{130}Xe/^{36}Ar and ^{84}Kr/^{36}Ar ratios and lower ^{22}Ne/^{36}Ar ratios compared to air, seawater, MORB and oceanic serpentinites could be the result of MORB alteration during the interaction with seawater on the seafloor and linked to the crystallisation of secondary minerals. At present there is insufficient mineralogical or age variations between the 12 samples analysed by heating to be able to judge if there is any relationship between these parameters and either the ^{130}Xe/^{36}Ar ratios or ^{130}Xe and ^{36}Ar concentrations.

Compared to mid-ocean ridge basalts, the AOC samples are hydrothermally altered resulting in the formation of secondary minerals and fluid inclusions. The 12 samples of this study analysed for total noble gas content are affected by low temperature alteration. They contain clays as the main secondary mineral in quantities >5% and do not contain amphiboles (Table 1). Clays are reported to fractionate noble gas elemental ratios, by preferential adsorption of the heavier noble gases (Podosek et al., 1981). In clay minerals, the ^{130}Xe/^{36}Ar and ^{84}Kr/^{36}Ar ratios are likely to be higher than in other materials. Therefore, it is plausible that the ^{130}Xe/^{36}Ar ratios and ^{84}Kr/^{36}Ar higher than MORB in the heated samples are related to the presence of clays.

It is possible that high ^{130}Xe/^{36}Ar ratios could also be related to the addition of a component having relatively high ^{130}Xe/^{36}Ar ratios that has been incorporated into the samples by mixing. For example, similarly high ^{130}Xe/^{36}Ar ratios have been reported in sediments (Matsuda and Nagao, 1986). It is important to note that any sedimentary signature would require ^{22}Ne/^{36}Ar and ^{84}Kr/^{36}Ar respectively higher and lower than the sediments reported by Matsuda and Nagao (1986) to account for the data observed in this study (Fig. 4). It is not necessary for direct incorporation of sediment *per se* as such a signature could

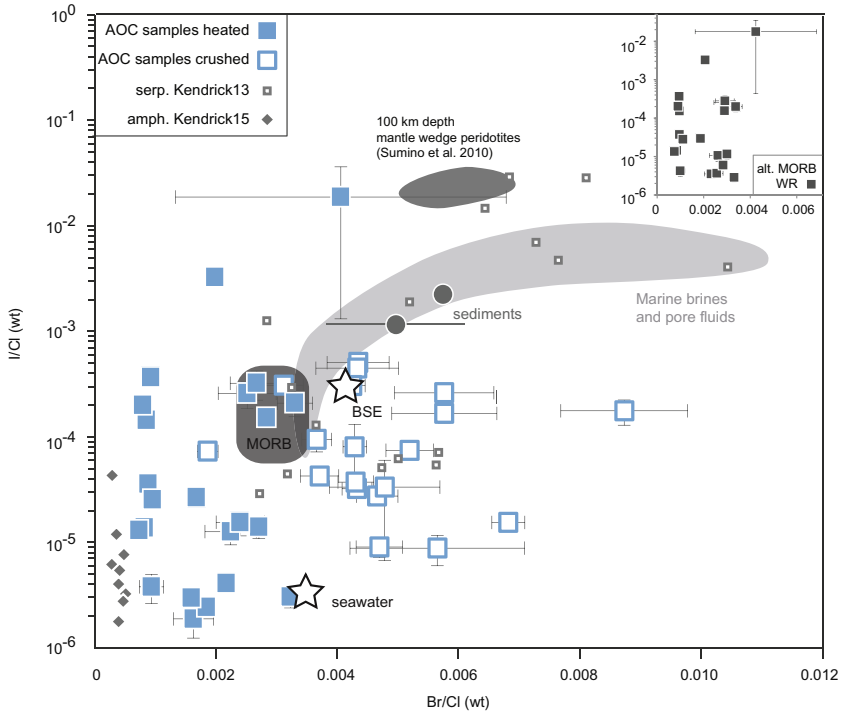

Fig. 6. Halogen mixing diagram, I/Cl versus Br/Cl. The AOC samples crushed data reflect the contents in fluid phases and the AOC samples heated data reflect the contents in the solid phases. Inset figure shows the bulk rock (=crushed + heated data) ratios which are similar to the heating results. The two seafloor marine sediments are from Muramatsu and Parr (1985), Suzuki and Hirai (1992), Yonezawa (1996) and Chai and Muramatsu (2007), the marine pore fluids are from Kastner et al. (1990), Martin et al. (1993), Muramatsu et al. (2001) and Fehn et al. (2006). BSE = Bulk Silicate Earth from Burgess et al. (2002), serp. Kendrick13 = oceanic serpentines of Kendrick et al. (2013b), amph. Kendrick15 = amphiboles from oceanic meta-gabbros (Kendrick et al., 2015), axial MORB glasses field from Déruelle et al. (1992), Jambon et al. (1995), Kendrick et al. (2012b).

originate from a fluid that interacted with sediment (i.e. marine pore fluid) before being trapped in fluid inclusions of AOC samples. This could explain the high $^{130}Xe/^{36}Ar$ ratios measured in the fluid inclusions (=crushed releases) of the samples shallower than 800–900 msb. The crushed samples deeper than 800–900 msb show lower $^{130}Xe/^{36}Ar$, closer to the seawater value. Thus for these samples, it is less likely that they are affected by a sedimentary contribution.

Finally, variable Xe/Ar and Kr/Ar ratios are found in fluids that have undergone phase separation during boiling (e.g. Kennedy et al., 1985). Such a process occurs in seafloor hydrothermal systems and could therefore influence the $^{130}Xe/^{36}Ar$ and $^{84}Kr/^{36}Ar$ of the fluids trapped in the samples. However in our study, because fluid inclusions are too small it has not been possible to investigate the degree of vapour-fill to determine if this process has occurred.

The K/Cl values of basalts should not be fractionated during magma processes because both K and Cl have similar silicate/melt partitioning coefficients. Variation in the K/Cl value of MORB has thus previously been used as a proxy for seawater assimilation (e.g. Michael and Cornell, 1998) and may also be related to the temperature of hydrothermal alteration. Sano et al. (2008) report that K/Cl values start to decrease with depth below 1100 msb in Hole 1256D reflecting higher temperature hydrothermal alteration (Fig. 2). In particular, K is taken up by basalts during low temperature alteration but is leached from basalts during high temperature reactions (Staudigel et al., 1996; Staudigel, 2003). Assimilation of seawater can also be excluded on the basis of halogen compositions because Br/Cl and I/Cl are not intermediate between MORB and seawater values (Fig. 6).

Two samples from depths shallower than 300 msb (Fig. 2) show elevated K/Cl, I/Cl values and I concentrations compared to MORB (Fig. 7). Although high I concentrations can occur in organic-rich sediments (Muramatsu and Hans Wedepohl, 1998), the two sediment values available in the literature have K/Cl ratios that are too low to explain this variation (Fig. 7A). Alternatively, high I/Cl may be attributable either to the formation of palagonite, which is known to increase I content (Kendrick et al., 2012b) or to bio-alteration effects, as I has a biophilic nature in marine environments (Elderfield and Truesdale, 1980). Indeed, sample 896-29R-64 exhibits unusual microscopic features (See Supplementary Material Fig. A4) that appear to resemble those associated with palagonite and bio-alteration. Bio-alteration has been previously detected in samples of the same ODP Hole 896A (Staudigel et al., 2008 and references therein). The other samples shallower than 800–900 msb have I/Cl ratios similar to or lower than MORB values and which negatively correlate with I (Figs. 2 and 7). It suggests that although I can slightly be lost from the samples, it is not highly affected by the low temperature alteration.

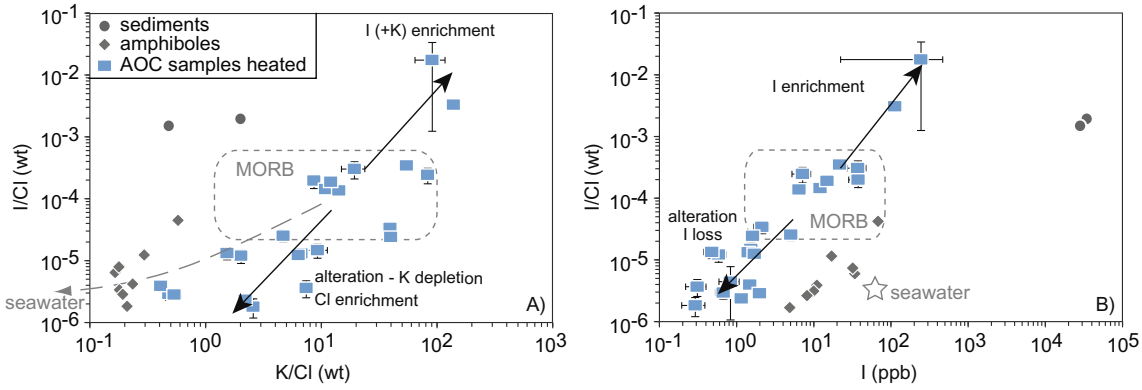

Fig. 7. I/Cl versus (A) K/Cl and (B) I. See the references for sediments, amphiboles and axial MORB glasses in legend of Fig. 6.

In samples deeper than 800–900 msb, with K/Cl and I/Cl values lower than MORB values (Figs. 2 and 7), I and K loss is interpreted to have occurred as these elements were leached from the basalts during higher temperature alteration processes. In addition, lower K/Cl, I/Cl and Br/Cl compared to MORB (Figs. 6, 7) could be partly related to the increase in Cl-rich amphibole content of the samples, a mineral that crystallises at high temperature during seafloor alteration in deeper portions of the AOC (Fig. 2). The relative compatibility of Cl in amphibole has been suggested previously (e.g. Magenheim et al., 1995; Hawthorne and Oberti, 2007; Barnes and Cisneros, 2012; Kendrick et al., 2015). In our samples, the K/Cl ratio is on average 30 when there is no amphibole in the sample and decreases to 1 in the three samples containing the most amphibole (Fig. 8). These samples also contain the highest Cl contents, as expected for their higher amphibole contents. The relationship between I/Cl, K/Cl and I content, implies that I is less compatible than Cl in amphibole and that I is removed from AOC samples during relatively high temperature alteration processes. Bromine is well-correlated with Cl (Fig. 5B) implying that it has a similar partitioning behaviour to Cl and that Br can also be incorporated into amphibole.

The higher Br/Cl ratios of crushed samples which are similar to the values of marine brines (Kendrick et al., 2013a) are likely to reflect the fluid phase contained in the altered basalts (Fig. 6). They may have been generated during phase separation of a saline fluid formed by seawater-basalt interaction (e.g. You et al., 1994; Svensen et al., 2001) and/or by Cl being slightly more incorporated than Br into the oceanic crust during the formation of hydrated secondary minerals such as amphibole.

5.3. Control on halogen and noble gas siting in the altered oceanic crust

During hydrothermal alteration, the Cl and Br compositions of the altered ocean crust appear to be related to amphibole crystallisation (Fig. 8), in which Cl and Br are more compatible relative to I. We compared the halogens contents with the main other minerals composing the samples and no other relationship has been observed. However,

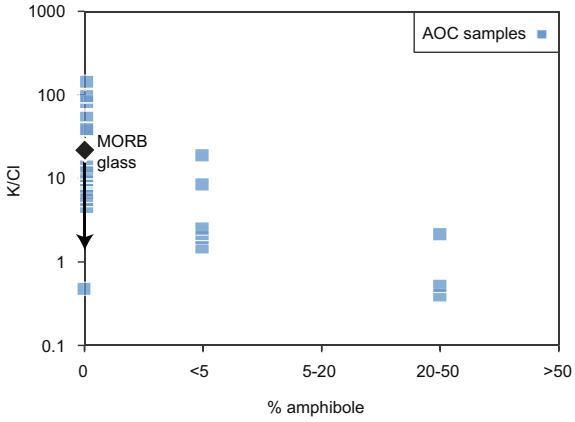

Fig. 8. K/Cl versus amphibole content, which crystallises at high temperature during the hydrothermal alteration of the samples.

it could be possible that halogens have some affinity with minor mineral phases, but the data are not available to test or quantify such a relationship. Also, assimilation of organic-rich sediment and/or interaction with a biological activity most likely contributes to increase I contents (and Br content to a lesser extent). Direct incorporation of seawater is not a major source of halogens in the samples (Figs. 6 and 7).

For the noble gases, we expect clays to preferentially adsorb ^{130}Xe relatively to ^{36}Ar on their surface in the AOC samples from depths shallower than 800–900 msb (Section 5.2.2). It is notable in Fig. 4 that mineral separates (including amphiboles) from oceanic meta-gabbros altered at high temperature, and therefore less likely to contain clays, have significantly lower $^{130}Xe/^{36}Ar$ ratios of <0.0005 (Kendrick et al., 2015). The crushing release of AOC samples altered at high temperature, i.e. those deeper than 800–900 msb, have also significantly lower $^{130}Xe/^{36}Ar$ ratios, <0.001. These findings suggest that highly fractionated $^{130}Xe/^{36}Ar$ values are mainly present in the samples altered by low temperature alteration, i.e. those shallower than 800–900 msb. Conversely, lower $^{130}Xe/^{36}Ar$ ratios are expected in deeper, amphibole-bearing samples (Fig. 2, Section 2.2). In addition, crushing of the deeper

samples released significantly more noble gases than the three shallower samples (Tables 1 and 2). Fluid inclusions are more abundant in the samples deeper than 800–900 msb, therefore it suggests that more noble gases are contained in the fluid inclusions of the deeper samples compared to the shallower samples.

5.4. Implications for heavy noble gas subduction and recycling into the mantle

In this study and previously by Staudacher and Allègre (1988), noble gas contents have been obtained for AOC samples from depths shallower than 800–900 msb (Tables 1 and 2). Deeper rocks show different lithologies, such as dykes and plutonic rocks and are altered at higher temperatures (Table 1, Fig. 2). Thus there are likely to be significant variations in noble gas contents as a function of depth in the oceanic crust. Acknowledging that the noble gas concentrations in this study are probably not representative of the whole oceanic crust, and that there is a paucity of data from the deeper layers, the following flux calculations have a degree of uncertainty and for this reason should be considered illustrative rather than definitive. Combining the noble gas data from this study ($n = 12$) with those from Staudacher and Allègre (1988) ($n = 8$), the average ^{36}Ar and ^{130}Xe of the AOC are $\sim 2 \times 10^{-9}$ cm^3 STP g^{-1} and $\sim 4 \times 10^{-12}$ cm^3 STP g^{-1} respectively (Table 4). These concentrations can be translated into noble gas fluxes available for subduction by making use of the following information: (1) an average convergence rate of 5 cm yr^{-1} (von Huene and Scholl, 1991; Jarrard, 2003); (2) a global arc length of 44,000 km (von Huene and Scholl, 1991; Jarrard, 2003); (3) an average ocean crust density of 2.8 g. cm^{-3} (Straub and Layne, 2003); and (4) a 6 km thick ocean crust. Based upon these parameters it is estimated that 3.7×10^{16} g yr^{-1} of oceanic crust is subducted. Therefore the annual fluxes of ^{36}Ar and ^{130}Xe trapped within the AOC entering the subduction zone are respectively $\sim 7 \times 10^7$ cm^3 STP yr^{-1} and $\sim 1.5 \times 10^5$ cm^3 STP yr^{-1} (Table 4).

Marine sediments and the serpentinisation of the underlying lithospheric mantle provide additional sources of volatiles available for subduction. Sea floor serpentinites and marine sediments respectively contain about 10 and 100 times more ^{36}Ar and ^{130}Xe than AOC samples (Table 4). Serpentinised ocean crust extending to a depth of 300 m (Barnes and Straub, 2010) has a ^{36}Ar subduction potential nearly equivalent to that of the AOC. By comparison, 400 m thick sediments yield ^{36}Ar and ^{130}Xe fluxes respectively $\sim$2 and 4 times higher than serpentines and AOC igneous rocks (Table 4).

Holland and Ballentine (2006) calculated that (5–8)$\times 10^7$ cm^3 STP ^{36}Ar yr^{-1} recycled over 4.5 Ga was needed to account for all of the ^{36}Ar in the upper mantle, depending on the extent of Ar degassing from the mantle. This value is similar to the total flux of ^{36}Ar available for subduction that we calculate for the AOC, but considerably less than the total flux of $\sim 30 \times 10^7$ cm^3 STP ^{36}Ar yr^{-1} if contributions from subducted serpentinites and sediments are included (Table 4).

5.5. Implications for halogen subduction and recycling into the mantle

5.5.1. Fluid phases versus solid phases

The different extraction methods employed in this study also make it possible to assess the partitioning of halogens between solid (heating) and fluid (crushing) phases. It is acknowledged that heating experiments also release halogens from any fluid inclusions remaining after crushing. Crushing experiments release fluid inclusions gases, but also noble gases trapped along grain boundaries and a portion of any contained in mineral lattices (Kendrick and Phillips, 2009). If we simplify by assuming that heating mainly releases the gases in solid phases and crushing data are dominated by fluid phases, then our results suggest that $\sim$90% of the halogens are incorporated in the mineral and/or volcanic matrix phases of the samples and $\sim$10% are contained in fluid phases. Sumino et al. (2010) reported subduction fluid-bearing noble gases and halogens with a marine pore-fluid signature from a depth of 100 km in exhumed mantle wedge peridotite. Altered ocean crust samples do not contain a component with such elevated I/Cl ratios as marine pore fluids. Assuming that I and Cl do not fractionate during the subduction process, it is unlikely that a fluid with the average AOC composition observed here can be the source of the subduction fluid reported by Sumino et al. (2010) (Fig. 6).

5.5.2. Consequence of the halogen heterogeneity with depth

The change in halogens ratios and concentrations with depth in the ocean crust has implications for the composition of slab fluids released during subduction (Fig. 2). Amphibole crystallisation is characteristic of hydrothermal alteration at deeper levels in the oceanic crust. Together with I loss during alteration, it effectively reduces the K/Cl and I/Cl values below that of MORB (Figs 2 and 7). High amounts of I have been recorded in back-arc basin basalts compared to Cl and Br, which are explained by the involvement of fluids released by breakdown of I-rich serpentinites (Kendrick et al., 2014). Our study shows that another potential source is the relatively I-enriched shallower layer of oceanic crust released into the mantle wedge during subduction. Moreover, depending on the geodynamic context and slab thermal regime, variations in the slab-derived fluid composition are expected. Using the example of water, the model of van Keken et al. (2011) suggests that in a cold subduction zone, the uppermost crust dehydrates below the volcanic front, whereas the entire lower oceanic crust can carry water to greater depths. If halogens behave similar to water, then the relatively low I/Cl and Br/Cl signatures of the deeper part of the AOC (>800–900 msb), compared to the shallower part (<800–900 msb), could be preferentially subducted deep into the mantle.

5.5.3. The halogen content of the altered oceanic crust

Although there are numerous measurements of Cl determinations of axial MORB glasses, there are relatively few analyses of altered ocean crust. Three values are given in Bonifacie et al. (2007) from ODP Hole 504B and 68 in

Table 4
Halogens and noble gases fluxes available for subduction.

	Concentrations					Available flux for subduction				
	^{36}Ar cm^3 STP g^{-1}	^{130}Xe cm^3 STP g^{-1}	Cl ppm	Br ppb	I ppb	^{36}Ar cm^3 STP yr^{-1}	^{130}Xe cm^3 STP yr^{-1}	Cl g yr^{-1}	Br g yr^{-1}	I g yr^{-1}
AOC igneous 3.7×10^{16} g yr^{-1}	$2^{+6}_{-1} \times 10^{-9}$ [a]	$4^{+16}_{-3} \times 10^{-12}$ [a]	253^{+436}_{-160} [b]	435^{+726}_{-272}	3^{+11}_{-2}	$7^{+22}_{-4} \times 10^{7}$	$1.5^{+5.9}_{-1.3} \times 10^{5}$	$9^{+16}_{-6} \times 10^{12}$	$16^{+27}_{-10} \times 10^{9}$	$1.1^{+4.1}_{-0.7} \times 10^{8}$
Oceanic Serpentinites[c] 1.8×10^{15} g yr^{-1}[d]	$40^{+123}_{-30} \times 10^{-9}$	$21^{+82}_{-17} \times 10^{-12}$	677^{+906}_{-387}	3178^{+6545}_{-2139}	751^{+6907}_{-677}	$7^{+20}_{-6} \times 10^{7}$	$0.4^{+1.3}_{-0.3} \times 10^{5}$	$1.3^{+1.7}_{-0.7} \times 10^{12}$	$6^{+12}_{-4} \times 10^{9}$	$13.9^{+128}_{-12.5} \times 10^{8}$
Marine sediments 2.5×10^{15} g yr^{-1}[e]	$74^{+9}_{-41} \times 10^{-9}$[f]	$148^{+300}_{-99} \times 10^{-12}$[f]	640[g]	-	-	$18^{+23}_{-10} \times 10^{7}$	$4^{+7}_{-2} \times 10^{5}$	1.6×10^{12}[g]		

[a] $n = 20$, including values from Staudacher and Allègre (1988).
[b] $n = 146$, including values from the literature (See Section 5.5.3 for explanations). For halogens, concentrations are calculated considering the heterogeneous distributions of the elements in the depth of oceanic crust with a limit at 800–900 msb.
[c] Calculated after the halogen and noble gas data of John et al. (2011) ($n = 5$) and Kendrick et al. (2013b) ($n = 17$).
[d] Assuming 300 m of serpentinites (Barnes and Straub, 2010).
[e] Considering 400 m of sediments (Straub and Layne, 2003).
[f] Calculated after the data of Staudacher and Allègre (1988) ($n = 3$) and Matsuda and Nagao (1986) ($n = 7$).
[g] Straub and Layne (2003).

Sano et al. (2008) for ODP Hole 1256D. Barnes and Cisneros (2012) analysed Cl in 50 gabbros, lavas and dykes from 7 sites, but their analyses are not precise below 100 ppm. Our finding that Cl contents are higher when amphibole is present is in agreement with the observations of Kendrick et al. (2015), Barnes and Cisneros (2012) and Ito et al. (1983). Using the data from this study (Table 4) and from the literature, depths shallower than 800–900 msb yield average $Cl = 98^{+192}_{-65}$ ppm ($n = 84$), whereas at depths greater than 800–900 msb, $Cl = 284^{+485}_{-179}$ ppm ($n = 62$) (the distributions are log-normal, see Supplementary Material Fig. C). Using these values and 6 km as the average thickness of oceanic crust, the total Cl content of the oceanic crust is estimated to be 253^{+436}_{-160} ppm. For comparison, this is higher than the un-weighted global average of 154^{+345}_{-106} ppm ($n = 146$) and about 3 times higher than previous estimates of Straub and Layne (2003) and John et al. (2011), that were calculated following the approach of Ito et al. (1983) by assuming that secondary amphibole is the major sink for seawater Cl. Ito et al. (1983) determined a Cl content of 50 ± 25 ppm, based on the hydrous mineral content of the oceanic crust. Bromine and I are also heterogeneous with depth. Bromine has a similar behaviour to Cl, and as a consequence is more abundant below 800–900 msb ($Br = 109^{+136}_{-60}$ ppb at depth < 800–900 msb, and $Br = 500^{+844}_{-314}$ ppb > 800–900 msb) and I is more abundant at shallower depths ($I = 6^{+32}_{-5}$ ppb < 800–900 msb; $I = 2^{+6}_{-1}$ ppb > 800–900 msb). Using these values, the weighted averages for ocean crust are estimated to be 435^{+726}_{-272} ppb Br and 3^{+11}_{-2} ppb I (Table 4).

5.5.4. Halogen flux available for subduction and recycling

The results obtained in this study can be used to obtain an improved estimate for the Cl flux available for subduction (Straub and Layne, 2003; John et al., 2011; Barnes and Cisneros, 2012) and provide the first estimates for Br and I. The available fluxes are estimated using the mean contents calculated in Section 5.5.3 (Table 4). The available Cl subduction flux contributed by the oceanic crust is $9^{+16}_{-6} \times 10^{12}$ g yr^{-1}. This is three times higher than the previous estimate of John et al. (2011) and five times the estimate of the Cl subduction flux of sediments (Straub and Layne, 2003). The available Cl subduction flux of the altered oceanic crust is potentially up to 7 times higher than the Cl flux contributed by the serpentinised oceanic mantle (calculated using halogen data from Kendrick et al., 2013b), assuming 300 m of serpentinite prior to subduction (Barnes and Straub, 2010). The available AOC subduction flux is also about ten times higher than the estimate of the Cl mantle flux released at mid-ocean ridges (Ito et al., 1983; Kagoshima et al., 2012). The Br flux of the oceanic crust is 2.5 times higher than the flux estimate from serpentinites (Table 4). In contrast, the I subduction flux for the oceanic crust is very low, 15 times lower than from the serpentinites (Table 4).

Our work suggests that the oceanic crust is an important Cl and Br reservoir which has the potential to provide a significant source of halogens for subduction to greater depths in the Earth's mantle (Table 4). A simple, first order

Table 5
Comparison of present day upper mantle halogen content with concentrations produced by AOC fluxing into the mantle over 3 Ga.

	Cl ppm	Br ppm	I ppm
Upper mantle today	1–8[a, b]	8[a]	0.8[c]
AOC to upper mantle in 3 Ga	27^{+45}_{-17}	47^{+79}_{-29}	$0.3^{+1}_{-0.2}$
AOC to whole mantle in 3 Ga	7^{+12}_{-4}	12^{+20}_{-8}	$0.08^{+0.2}_{-0.05}$

[a] Jambon et al. (1995).
[b] Bonifacie et al. (2008).
[c] Déruelle et al. (1992).

calculation gives an indication of the potential of AOC halogens to be recycled in the deep mantle. By combining the estimates of the present day AOC halogen flux with the annual plate subduction rate determined earlier (3.7×10^{16} g yr^{-1}) for the last 3 Ga (the time assumed to be when plate tectonics started, e.g. Shirey and Richardson, 2011), in a mantle with a starting halogen concentration of zero, then the mantle would have accumulated ~30 ppm Cl, ~50 ppb Br and ~0.3 ppb I. If the AOC was fluxed into the whole mantle these concentrations would be ~3 times lower (Table 5). Current estimates for MORB-source mantle are based on limited data but suggest 1–8 ppm Cl, 8 ppb Br, and 0.8 ppb I (Déruelle et al., 1992; Jambon et al., 1995; Bonifacie et al., 2008) (Table 5). The calculation assumes that all the halogens in the ocean crust are returned to the mantle in the down-going slabs at subduction zones and are therefore maximum possible estimates. It also takes no account of any loss of halogens from the mantle by degassing at mid-ocean ridges, previously suggested as being negligible (Kendrick et al., 2012b). These assumptions aside, and recognising the influence from partial loss of halogens by dehydration in subduction zones (van Keken et al., 2011), this calculation is illustrative in demonstrating that sufficient Cl and Br can potentially be delivered by subduction over the last 3 Ga to account for mantle source compositions.

6. SUMMARY

To better understand the deep cycling of noble gases and halogens in the Earth, we analysed the noble gases and halogens in AOC samples from altered Pacific Ocean crust ranging from 6.9 to 170 Ma. Crushing experiments and heating experiments allow the determination of the composition of fluid phases and the solid phases respectively.

(1) The crushing experiments and heating experiments in AOC samples show similar noble gases signatures, except for ^{4}He and ^{40}Ar, which are affected by radioactive decay of U, Th and K in the samples matrices. All samples show a strong atmospheric overprint most likely introduced by seawater–rock interaction during alteration. Furthermore, ^{130}Xe/^{36}Ar ratios extend up to 15 times the seawater value. High ^{130}Xe/^{36}Ar ratios are likely related to both the presence of clays which adsorb heavier noble gases, and the presence of fluid inclusions containing a marine pore fluid composition. Another possibility, considered less likely, is noble gas fractionation related to phase separation during boiling prior to fluid inclusion trapping.
(2) On average ~90% of the total halogens are released during the heating experiments showing the dominant source of the halogens to be within mineral phases. The I/Cl ratios of the AOC samples vary by up to four orders of magnitude, although many samples retain their original MORB values. Deviation from MORB values can be explained by an interaction with sediments or by biological activity increasing I/Cl (shallowest samples), and crystallisation of amphibole during the high temperature alteration on the seafloor leading to lower I/Cl values and Br/Cl (samples deeper than 800–900 msb). In addition, I is probably leached from the samples during the alteration.
(3) The results highlight the different geochemical behaviour of noble gases and halogens during alteration of ocean crust. There is no obvious relationship between noble gas and halogen compositions related to age of crust or its geographical location. Part of the differences reflects a different mineralogical control. In particular, the formation of Cl-bearing amphibole during high temperature alteration at depths higher than 800–900 msb influences the halogen contents. At depths shallower than 800–900 msb, during the low temperature alteration, the noble gas composition is probably related to clays crystallisation.
(4) The Br/Cl values of solid and fluid phases of AOC samples are lower and higher than seawater respectively. Together with the highly variable I/Cl value, this means the halogen signature of the AOC samples is distinct from that of serpentinites, MORB, seawater and marine pore fluids.
(5) The oceanic crust and serpentinites are similar sized reservoirs for ^{36}Ar subduction, but are likely smaller reservoirs than the sediments. The ocean crust represents a potential reservoir with a capacity to dominate the Cl and Br fluxes into the mantle. In contrast, the I subduction flux of the oceanic crust is more than an order of magnitude lower than the amount that can be contributed from oceanic serpentinites.

ACKNOWLEDGMENTS

We thank Bridget Moorsom, Bev Clementson, Dave Blagburn and John Cowpe for assistance in the Manchester noble gas labs, John Waters for the XRD measurements and Steve Stockley for preparation of thin sections. Keisuke Nagao is thanked for assistance in the Tokyo lab. We acknowledge the assistance of Kenji Notsu and the Gulf Coast Repository (Texas) of the Integrated Ocean Drilling Program for providing the samples. This work was supported by NERC grant NE/G018014/1, and ERC grant ERC-267692 to CJB and RB, Sasagawa Scientific Research Grant from the Japan Science Society and COE program of The

University of Tokyo to AS, and MEXT/JSPS KAKENHI Grant Numbers 23340169 and 24109702, the Sumitomo Foundation and Inamori Foundation to HS. Colin Jackson and two anonymous reviewers are thanked for their constructive reviews which helped to improve this manuscript.

APPENDIX A. SUPPLEMENTARY DATA

Supplementary data associated with this article can be found, in the online version, at http://dx.doi.org/10.1016/j.gca.2016.03.014.

REFERENCES

Allègre C. J., Staudacher T., Sarda P. and Kurz M. (1983) Constraints on evolution of Earth's mantle from rare gas systematics. *Nature* **303**, 762–766.

Alt J. C., Anderson T. F., Bonnell L. and Muehlenbachs K. (1989) Mineralogy, chemistry, and stable isotopic compositions of hydrothermally altered sheeted dikes: ODP Hole 504B, Leg 111. In *Proc. ODP, Sci. Results 111: College Station, TX (Ocean Drilling Program)* (ed. H. Sakai) (ed. K. Becker), pp. 27–40. http://dx.doi.org/10.2973/odp.proc.sr.111.114.1989.

Alt J. C., Kinoshita H. and Stokking L. B. (1993) *Proc. ODP, Init. Repts. 148: College Station, TX (Ocean Drilling Program)*. http://dx.doi.org/10.2973/odp.proc.ir.148.1993.

Alt J. C., Laverne C., Coggon R. M., Teagle D. A. H., Banerjee N. R., Morgan S., Smith-Duque C. E., Harris M. and Galli L. (2010) Subsurface structure of a submarine hydrothermal system in ocean crust formed at the East Pacific Rise, ODP/IODP Site 1256. *Geochem. Geophys. Geosyst.* **11**, Q10010.

Anderson R. N., Honnorez J. and Becker K. (1985) *DSDP, Init. Repts. 83: College Station, TX (Ocean Drilling Program)*. http://dx.doi.org/10.2973/dsdp.proc.83.1985.

Ballentine C. J. and Barfod D. N. (2000) The origin of air-like noble gases in MORB and OIB. *Earth Planet. Sci. Lett.* **180**, 39–48.

Ballentine C. J. and Holland G. (2008) What CO_2 well gases tell us about the origin of noble gases in the mantle and their relationship to the atmosphere. *Philos. Trans. Roy. Soc. A* **366**, 4183–4203.

Ballentine C. J., Marty B., Sherwood Lollar. B. and Cassidy M. (2005) Neon isotopes constrain convection and volatile origin in the Earth's mantle. *Nature* **433**, 33–38.

Barnes J. D. and Cisneros M. (2012) Mineralogical control on the chlorine isotope composition of altered oceanic crust. *Chem. Geol.* **326–327**, 51–60.

Barnes J. D. and Straub S. M. (2010) Chorine stable isotope variations in Izu Bonin tephra: implications for serpentinite subduction. *Chem. Geol.* **272**, 62–74.

Becker K. and Sakai H. (1988) *Proc. ODP, Init. Repts. 111: College Station, TX (Ocean Drilling Program)*. http://dx.doi.org/10.2973/odp.proc.ir.111.1988.

Böhlke J. K. and Irwin J. J. (1992) Laser microprobe analyses of noble gas isotopes and halogens in fluid inclusions: analyses of microstandards and synthetic inclusions in quartz. *Geochim. Cosmochim. Acta* **56**, 187–201.

Bonifacie M., Jendrzejewski N., Agrinier P., Coleman M., Pineau F. and Javoy M. (2007) Pyrohydrolysis-IRMS determination of silicate chlorine stable isotope compositions. Application to oceanic crust and meteorite samples. *Chem. Geol.* **242**, 187–201.

Bonifacie M., Jendrzejewski N., Agrinier P., Humler E., Coleman M. and Javoy M. (2008) The chlorine isotope composition of Earth's mantle. *Science* **319**, 1518–1520.

Brandenburg J. P., Hauri E. H., van Keken P. E. and Ballentine C. J. (2008) A multiple-system study of the geochemical evolution of the mantle with force-balanced plates and thermochemical effects. *Earth Planet. Sci. Lett.* **276**, 1–13.

Burgess R., Layzelle E., Turner G. and Harris J. W. (2002) Constraints on the age and halogen composition of mantle fluids in Siberian coated diamonds. *Earth Planet. Sci. Lett.* **197**, 193–203.

Burnard P., Graham D. and Turner G. (1997) Vesicle-specific noble gas analyses of "popping rock": implications for primordial noble gases in Earth. *Science* **276**, 568–571.

Chai J. Y. and Muramatsu Y. (2007) Determination of bromine and iodine in twenty-three geochemical reference materials by ICP-MS. *Geostand. Geoanal. Res.* **31**, 143–150.

Déruelle B., Dreibus G. and Jambon A. (1992) Iodine abundances in oceanic basalts: implications for Earth dynamics. *Earth Planet. Sci. Lett.* **108**, 217–227.

Dick H. J. B., Erzinger J. and Stokking L. B. (1992) *Proc. ODP, Init. Repts. 140: College Station, TX (Ocean Drilling Program)*. http://dx.doi.org/10.2973/odp.proc.ir.140.1992.

Elderfield H. and Truesdale V. W. (1980) On the biophilic nature of iodine in seawater. *Earth Planet. Sci. Lett.* **50**, 105–114.

Fehn U., Lu Z. and Tomaru H. (2006) Data report: 129I/I ratios and halogen concentrations in pore water of the Hydrate Ridge and their relevance for the origin of gas hydrates: a progress report. In *Proc. ODP, Sci. Results 204* (eds. A. M. Tréhu, G. Bohrmann, M. E. Torres and F. S. Colwell), College Station, TX (Ocean Drilling Program), pp. 1–25. doi:10.2973/odp.proc.sr.204.107.2006.

Gao Y., Vils F., Cooper K. M., Banerjee N., Harris M., Hoefs J., Teagle D. A. H., Casey J. F., Elliott T., Laverne C., Alt J. C. and Muehlenbachs K. (2012) Downhole variation of lithium and oxygen isotopic compositions of oceanic crust at East Pacific Rise, ODP Site 1256. *Geochem. Geophy. Geosyst.* **13**, Q10001.

Hawthorne F. C. and Oberti R. (2007) Amphiboles: crystal chemistry. *Rev. Mineral. Geochem.* **67**, 1–54.

Hohenberg C. M. (1967) I-Xe dating of the Shallowater achondrite. *Earth Planet. Sci. Lett.* **3**, 357–362.

Holland G. and Ballentine C. J. (2006) Seawater subduction controls the heavy noble gas composition of the mantle. *Nature* **441**, 186–191.

Holland G., Cassidy M. and Ballentine C. J. (2009) Meteorite Kr in Earth's mantle suggests a late accretionary source for the atmosphere. *Science* **326**, 1522–1525.

Ito E., Harris D. M. and Anderson, Jr, A. T. (1983) Alteration of oceanic crust and geologic cycling of chlorine and water. *Geochim. Cosmochim. Acta* **47**, 1613–1624.

Jackson C. R. M., Parman S. W., Kelley S. P. and Cooper R. F. (2013) Noble gas transport into the mantle facilitated by high solubility in amphibole. *Nat. Geosci.* **6**, 562–565.

Jackson C. R. M., Parman S. W., Kelley S. P. and Cooper R. F. (2015) Light noble gas dissolution into ring structure-bearing materials and lattice influences on noble gas recycling. *Geochim. Cosmochim. Acta* **159**, 1–15.

Jambon A., Déruelle B., Dreibus G. and Pineau F. (1995) Chlorine and bromine abundance in MORB: the contrasting behaviour of the Mid-Atlantic Ridge and East Pacific Rise and implications for chlorine geodynamic cycle. *Chem. Geol.* **126**, 101–117.

Jarrard R. D. (2003) Subduction fluxes of water, carbon dioxide, chlorine, and potassium. *Geochem. Geophy. Geosyst.* **4**, 8905.

John T., Scambelluri M., Frische M., Barnes J. D. and Bach W. (2011) Dehydration of subducting serpentinite: implications for halogen mobility in subduction zones and the deep halogen cycle. *Earth Planet. Sci. Lett.* **308**, 65–76.

Johnson L. H., Burgess R., Turner G., Milledge H. J. and Harris J. W. (2000) Noble gas and halogen geochemistry of mantle fluids: comparison of African and Canadian diamonds. *Geochim. Cosmochim. Acta* **64**, 717–732.

Jourdan F., Verati C. and Féraud G. (2006) Intercalibration of the Hb3gr $^{40}Ar/^{39}Ar$ dating standard. *Chem. Geol.* **231**, 177–189.

Kagoshima T., Takahata N., Jung J., Amakawa H., Kumagai H. and Sano Y. (2012) Estimation of sulfur, fluorine, chlorine and bromine fluxes at Mid Ocean Ridges using a new experimental crushing and extraction method. *Geochem. J.* **46**, e21–e26.

Kaneoka I. (1983) Noble gas constraints on the layered structure of the mantle. *Nature* **302**, 698–700.

Kastner M., Elderfield H., Martin J. B., Suess E., Kvenvolden K. A. and Garrison R. E. (1990) Diagenesis and interstitial-water chemistry at the Peruvian continental margin—major constituents and strontium isotopes. In *Proc. ODP, Sci. Results 112* (eds. E. Suess, R. von Huene, et al.), College Station, TX (Ocean Drilling Program), 413–440. doi:10.2973/odp.proc.sr.112.144.1990.

Kelley K. A., Plank T., Ludden J. and Staudigel H. (2003) Composition of altered oceanic crust at ODP Sites 801 and 1149. *Geochem. Geophy. Geosyst.* **4**, 8910.

Kendrick M. A. (2012) High precision Cl, Br and I determinations in mineral standards using the noble gas method. *Chem. Geol.* **292–293**, 116–126.

Kendrick M. A. and Phillips D. (2009) New constraints on the release of noble gases during in vacuo crushing and application to scapolite Br–Cl–I and $^{40}Ar/^{39}Ar$ age determinations. *Geochim. Cosmochim. Acta* **73**, 5673–5692.

Kendrick M. A., Scambelluri M., Honda M. and Phillips D. (2011) High abundances of noble gas and chlorine delivered to the mantle by serpentinite subduction. *Nat. Geosci.* **4**, 807–812.

Kendrick M. A., Kamenetsky V. S., Phillips D. and Honda M. (2012) Halogen systematics (Cl, Br, I) in mid-ocean ridge basalts: a Macquarie island case study. *Geochim. Cosmochim. Acta* **81**, 82–93.

Kendrick M. A., Arculus R., Burnard P. and Honda M. (2013a) Quantifying brine assimilation by submarine magmas: examples from the Galápagos Spreading Centre and Lau Basin. *Geochim. Cosmochim. Acta* **123**, 150–165.

Kendrick M. A., Honda M., Pettke T., Scambelluri M., Phillips D. and Giuliani A. (2013b) Subduction zone fluxes of halogens and noble gases in seafloor and forearc serpentinites. *Earth Planet. Sci. Lett.* **365**, 86–96.

Kendrick M. A., Arculus R. J., Danyushevsky L. V., Kamenetsky V. S., Woodhead J. D. and Honda M. (2014) Subduction-related halogens (Cl, Br and I) and H_2O in magmatic glasses from Southwest Pacific Backarc Basins. *Earth Planet. Sci. Lett.* **400**, 165–176.

Kendrick M. A., Honda M. and Vanko D. A. (2015) Halogens and noble gases in Mathematician Ridge meta-gabbros, NE Pacific: implications for oceanic hydrothermal root zones and global volatile cycles. *Contrib. Mineral. Petrol.* **170**, 1–20.

Kennedy B. M., Lynch M. A., Reynolds J. H. and Smith S. P. (1985) Intensive sampling of noble gases in fluids at Yellowstone I. Early overview of the data, regional patterns. *Geochim. Cosmochim. Acta* **49**, 1251–1261.

Kumagai H., Dick H. J. B. and Kaneoka I. (2003) Noble gas signatures of abyssal gabbros and peridotites at an Indian Ocean core complex. *Geochem. Geophy. Geosyst.* **4**, 9107.

Lancelot Y. and Larson R. L. (1990) *Proc. ODP, Init. Repts. 129: College Station, TX (Ocean Drilling Program)*. http://dx.doi.org/10.2973/odp.proc.ir.129.1990.

Lehnert K., Su Y., Langmuir C. H., Sarbas B. and Nohl U. (2000) A global geochemical database structure for rocks. *Geochem. Geophy. Geosyst.* **1**, 1–14.

Magenheim A. J., Spivack A. J., Michael P. J. and Gieskes J. M. (1995) Chlorine stable isotope composition of the oceanic crust: implications for Earth's distribution of chlorine. *Earth Planet. Sci. Lett.* **131**, 427–432.

Marrocchi Y., Marty B., Reinhardt P. and Robert F. (2011) Adsorption of xenon ions onto defects in organic surfaces: implications for the origin and the nature of organics in primitive meteorites. *Geochim. Cosmochim. Acta* **75**, 6255–6266.

Martin J. B., Gieskes J. M., Torres M. and Kastner M. (1993) Bromine and iodine in Peru margin sediments and pore fluids: implications for fluid origins. *Geochim. Cosmochim. Acta* **57**, 4377–4389.

Matsuda J. and Nagao K. (1986) Noble gas abundances in a deep-sea sediment core from eastern equatoral pacific. *Geochem. J.* **20**, 71–80.

Matsuda J., Matsumoto T., Sumino H., Nagao K., Yamamoto J., Miura Y., Kaneoka I., Takahata N. and Sano Y. (2002) The $^{3}He/^{4}He$ ratio of the new internal He Standard of Japan (HESJ). *Geochem. J.* **36**, 191–195.

Michael P. J. and Cornell W. C. (1998) Influence of spreading rate and magma supply on crystallization and assimilation beneath mid-ocean ridges: evidence from chlorine and major element chemistry of mid-ocean ridge basalts 356. *J. Geophys. Res.* **103** (18), 325-318.

Moreira M. (2013) Noble gas constraints on the origin and evolution of Earth's volatiles. *Geochem. Perspect.* **2**, 229–403.

Moreira M., Kunz J. and Allègre C. J. (1998) Rare gas systematics in popping rock: isotopic and elemental compositions in the upper mantle. *Science* **279**, 1178–1183.

Moreira M., Blusztajn J., Curtice J., Hart S., Dick H. and Kurz M. D. (2003) He and Ne isotopes in oceanic crust: implications for noble gas recycling in the mantle. *Earth Planet. Sci. Lett.* **216**, 635–643.

Mukhopadhyay S. (2012) Early differentiation and volatile accretion recorded in deep-mantle neon and xenon. *Nature* **486**, 101–104.

Muramatsu Y. and Hans Wedepohl. K. (1998) The distribution of iodine in the earth's crust. *Chem. Geol.* **147**, 201–216.

Muramatsu Y. and Parr R. M. (1985) *IAEA/RL/128: survey of currently available reference materials for use in connection with the determination of trace elements in biological and environmental materials*. Int. Atom. Energ, Agency, Vienna.

Muramatsu Y., Fehn U. and Yoshida S. (2001) Recycling of iodine in fore-arc areas: evidence from the iodine brines in Chiba, Japan. *Earth Planet. Sci. Lett.* **192**, 583–593.

O'Nions R. K. and Oxburgh E. R. (1983) Heat and helium in the Earth. *Nature* **306**, 429–431.

Osawa T. (2004) A new correction technique for mass interferences by $^{40}Ar^{++}$ and CO_2^{++} during isotope analysis of a small amount of Ne. *J. Mass Spectrom. Soc. Jpn* **52**, 230–232.

Parai R. and Mukhopadhyay S. (2015) The evolution of MORB and plume mantle volatile budgets: constraints from fission Xe isotopes in Southwest Indian Ridge basalts. *Geochem. Geophy. Geosyst.* **16**, 719–735.

Plank T., Ludden J.N., Escutia C., et al. (2000) Proc. ODP, Init. Repts. 185: College Station, TX (Ocean Drilling Program). doi:10.2973/odp.proc.ir.185.2000.

Podosek F. A., Bernatowicz T. J. and Kramer F. E. (1981) Adsorption of xenon and krypton on shales. *Geochim. Cosmochim. Acta* **45**, 2401–2415.

Porcelli D. and Ballentine C. J. (2002) Models for the distribution of terrestrial noble gases and the evolution of the atmosphere. *Rev. Mineral. Geochem.* **47**, 411–480.

Porcelli D. and Wasserburg G. J. (1995) Mass transfer of helium, neon, argon, and xenon through a steady-state upper mantle. *Geochim. Cosmochim. Acta* **59**, 4921–4937.

Roddick J. C. (1983) High precision intercalibration of ^{40}Ar-^{39}Ar standards. *Geochim. Cosmochim. Acta* **47**, 887–898.

Sano Y. and Fischer T. P. (2013) The analysis and interpretation of noble gases in modern hydrothermal systems. In *The Noble Gases as Geochemical Tracers* (ed. P. Burnard). Springer, Berlin Heidelberg, pp. 249–317.

Sano T., Miyoshi M., Ingle S., Banerjee N. R., Ishimoto M. and Fukuoka T. (2008) Boron and chlorine contents of upper oceanic crust: basement samples from IODP Hole 1256D. *Geochem. Geophys. Geosyst.* **9**, Q12O15.

Schilling J. G., Bergeron M. B. and Evans R. (1980) Halogens in the mantle beneath the North Atlantic. *Phil. Trans. R. Soc. Lond. A* **297**, 147–178.

Shirey S. B. and Richardson S. H. (2011) Start of the Wilson cycle at 3 Ga shown by diamonds from subcontinental mantle. *Science* **333**, 434–436.

Staudacher T. and Allègre C. J. (1988) Recycling of oceanic crust and sediments: the noble gas subduction barrier. *Earth Planet. Sci. Lett.* **89**, 173–183.

Staudigel H. (2003) Hydrothermal alteration processes in the oceanic crust. In *Treatise of Geochemistry* (eds. H. Holland and K. Turekian), pp. 511–537.

Staudigel H., Plank T., White W. and Schmincke H.-U. (1996) Geochemical fluxes during seafloor alteration of the basaltic upper crust: DSDP Sites 417 and 418. In *Subduction: Top to Bottom* (ed. G. E. Bebout). Geophys. Monogr. Ser., AGU, Washington, D.C., pp. 19–38.

Staudigel H., Furnes H., McLoughlin N., Banerjee N. R., Connell L. B. and Templeton A. (2008) 3.5 billion years of glass bioalteration: volcanic rocks as a basis for microbial life? *Earth-Sci. Rev.* **89**, 156–176.

Straub S. M. and Layne G. D. (2003) The systematics of chlorine, fluorine, and water in Izu arc front volcanic rocks: implications for volatile recycling in subduction zones. *Geochim. Cosmochim. Acta* **67**, 4179–4203.

Stuart M., Turner G. and Taylor R. (1994) He–Ar isotope systematics of fluid inclusions: resolving mantle and crustal contributions to hydrothermal fluids. In *Noble Gas Geochemistry and Cosmochemistry* (ed. J. Matsuda). Terra Scientific Publishing Company, Tokyo, pp. 261–277.

Sumino H., Nagao K. and Notsu K. (2001) Highly sensitive and precise measurement of helium isotopes using a mass spectrometer with double collector system. *J. Mass. Spectrom. Soc. Jpn* **49**, 61–68.

Sumino H., Burgess R., Mizukami T., Wallis S. R., Holland G. and Ballentine C. J. (2010) Seawater-derived noble gases and halogens preserved in exhumed mantle wedge peridotite. *Earth Planet. Sci. Lett.* **294**, 163–172.

Suzuki S. and Hirai S. (1992) Multielement determination in marine sediment reference material by instrumental neutron activation analysis. *Jpn Analyst* **41**, 163–166.

Svensen H., Jamtveit B., Banks D. A. and Austrheim H. (2001) Halogen contents of eclogite facies fluid inclusions and minerals: caledonides, western Norway. *J. Metamorph. Geol.* **19**, 165–178.

Teagle D. A. H., Alt J. C., Umino S., Miyashita S., Banerjee N. R., Wilson D. S. and the Expedition 309/312 Scientists (2006) Proc. IODP 309/312: Washington, DC (Integrated Ocean Drilling Program Management International, Inc.). doi:10.2204/iodp.proc.309312.2006.

Turner G. (1965) Extinct iodine 129 and trace elements in chondrites. *J. Geophys. Res.* **70**, 5433–5445.

van der Hilst R. D., Widiyantoro S. and Engdahl E. R. (1997) Evidence for deep mantle circulation from global tomography. *Nature* **386**, 578–584.

van Keken P. E. and Ballentine C. J. (1999) Dynamical models of mantle volatile evolution and the role of phase transitions and temperature-dependent rheology. *J. Geophys. Res.* **104**, 7137–7151.

van Keken P. E., Hacker B. R., Syracuse E. M. and Abers G. A. (2011) Subduction factory: 4. Depth-dependent flux of H_2O from subducting slabs worldwide. *J. Geophys. Res.* **116**, B01401.

von Huene R. and Scholl D. W. (1991) Observations at convergent margins concerning sediment subduction, subduction erosion, and the growth of continental crust. *Rev. Geophys.* **29**, 279–316.

Wilson D. S., Teagle D. A. H. and Acton G. D. (2003) *Proc. ODP, Init. Repts. 206: College Station, TX (Ocean Drilling Program)*. http://dx.doi.org/10.2973/odp.proc.ir.206.2003.

Yonezawa C. (1996) Multi-element determination by a cold neutron-induced prompt gamma-ray analysis. *Anal. Sci.* **12**, 605–613.

You C. F., Butterfield D. A., Spivack A. J., Gieskes J. M., Gamo T. and Campbell A. J. (1994) Boron and halide systematics in submarine hydrothermal systems: effects of phase separation and sedimentary contributions. *Earth Planet. Sci. Lett.* **123**, 227–238.

Associate editor: Jun-ichiro Ishibashi